Towards landing a deep-stalled flying-wing in a powered flat spin: a proof of concept

Aerospace Engineering MSc Thesis

Matteo Barbera | 2022

Technical University of Delft

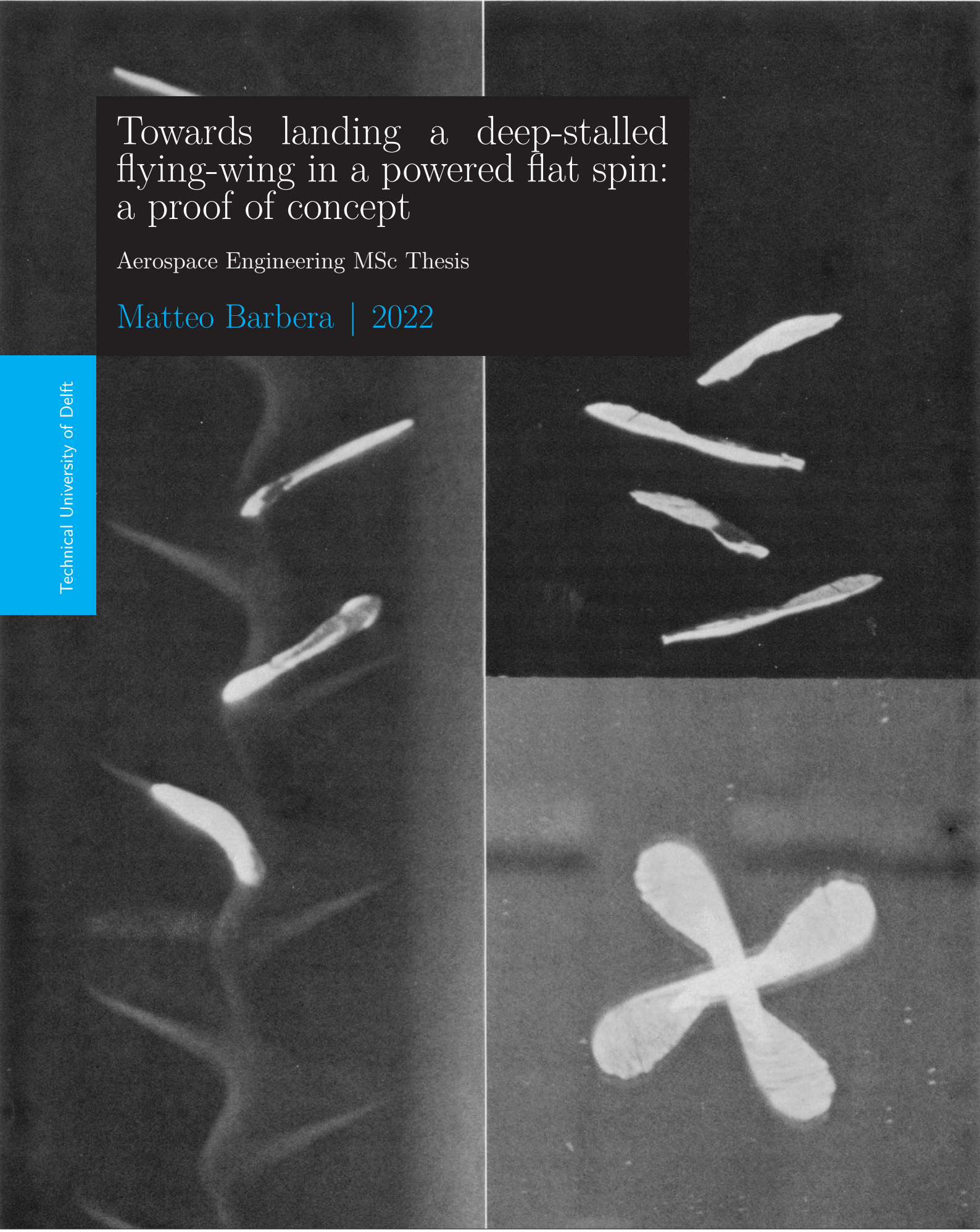

TU Delft Delft University of Technology

Challenge the future

MSc Thesis in Aerospace

Towards landing a deep-stalled flying-wing in a powered flat spin: a proof of concept

Matteo Barbera

November 30, 2022

This thesis was submitted to the Technical University of Delft in partial fulfillment of the requirements for the degree of Master of Science in Aerospace Engineering

Supervisors:

Christophe de Wagter
Bart Remes

Matteo Barbera: *Towards landing a deep-stalled flying-wing in a powered flat spin: a proof of concept* (November 30, 2022)

Supervisors: Christophe de Wagter
Bart Remes

Contents

List of Figures

List of Tables

Acknowledgements

The MSc Thesis is seen as the largest individual assignment of the study program, but this manuscript could never have been realized without the help and support of so many people, all of whom deserve my heartfelt thanks. To my supervisors, Christophe and Bart, thank you for always pushing me in the right direction and persevering with me throughout this project. To Erik, thank you for being forever willing to tackle any hardware problem I threw your way and solve it with what can sometimes only be described as dark magic. To Alessandro, thank you for always being willing to listen to my everyday problem and show me just how much my solutions could be improved. To my friends and peers, thank you for listening to my hardships and sharing your own, no matter how different our issues we were always the better for it. To my family, thank you for supporting me every step of the way. And finally to Özge, thank you for everything, I could not have done it without you.

Introduction

Unmanned aerial vehicles (UAVs) are expected to transition into many commercial markets in the coming years. Albeit still being an emerging technology, many forecasts maintain a very positive outlook on the drone market, some estimating it to double between 2018 and 2024 [8], and others expecting the market to bring EUR 10 billions per year by 2035 and EUR 15 billions by 2050 [9]. Europe's SESAR Joint Undertaking lists a number of challenges that will need to be addressed as the technology begins to be implemented in the civilian sector, namely the integration of UAVs in the current airspace, public safety in urban markets, improved Detect and Avoid technologies and data communication, to enable safe, reliable, Beyond Visual Line of Sight (BVLOS) missions [9].

While the applications of smaller drones, or Micro Air Vehicles (MAVs), extend to many different industry sectors, it is no secret that the technology continues to suffer serious limitations when it comes to flight time and payload capacity, as they often rely on batteries for power. MAVs typically sport a flight time of around 10 to 90 minutes, depending on their configuration and payload [10]. Multi-rotor MAVs are one of the most common drone configurations, their popularity stemming from their mechanical simplicity and hovering abilities, the latter proving extremely valuable, especially in urban environments, where the space for take-off and landing is often constrained [11]. Multi-rotors weighing around 1 kg, however, struggle to achieve 20 minutes of flight time, significantly limiting their applications [12]. Hybrid configurations attempt to combine the aerodynamic efficiency of fixed-wing drones, while still taking advantage of the VTOL capabilities of multi-rotors, and is the configuration of choice of many emerging drone manufacturing companies, such as Avy[1], Wingcopter[2], and Eloy Air[3]. These types of drones incur penalties in terms of payload or endurance, due to the added weight and worse aerodynamic profile caused by the extra lifting rotors [11]. Crucially, these payload and endurance penalties become more and more significant as the size of the drone decreases. Given a smaller diameter, a propeller must spin faster in order to produce the same thrust, causing the current draw of the motors to increase. A higher current draw for the same thrust results in a lower propeller efficiency, placing lightweight drones at a distinct disadvantage. Transforming light, flying wing platforms into a hybrid configuration to add VTOL capabilities becomes untenable for smaller platforms. A different solution must therefore be found.

This thesis will explore a new landing method for a flying-wing drone configuration that will allow the MAV to land vertically, without requiring hardware dedicated only to the take-off and landing phases. Since these flight phases only make up a small portion of the flight envelope, there is potential for extending the flight time and/or payload capabilities for this type of drone by taking full advantage of its aerodynamic efficiency, while still being capable of landing in enclosed environments. The landing is inspired by the flight of maple seeds, and will be achieved by inducing a flat spin and developing a controller that will manipulate the position and plane of rotation of the drone using its standard actuators, allowing the pilot to perform a controlled vertical descent. The report is structured as follows: Part I delves into the relevant literature and state of the art, and outlines the research goal. Part II presents the research and conclusions of this thesis in a scientific article format, and Part III describes in more detail the engineering challenges encountered throughout the project and their solutions.

[1] https://www.avy.eu/
[2] https://wingcopter.com/
[3] https://elroyair.com/

I

Literature Review

1
Literature Review

In this section a detailed analysis of the relevant literature is given. Section 1.1 explains the research that has been conducted on samara seeds, which inspired the work proposal of this thesis. Section 1.2 discusses unconventional MAV configurations similar to the eventual product of the project proposal, configurations that also attempt to emulate the flight of samaras. In the last part of this literature review, Section 1.3 delves into the work that has been conducted with regards to other rotating platforms that may be of interest. The section is concluded by a short synthesis of the state-of-the-art in Section 1.4.

1.1. Mechanics of Samaras

In an article for *Science*, Pfeifer et al. stated that "biological organisms have evolved to perform and survive in a world characterized by rapid changes, high uncertainty, indefinite richness, and limited availability of information" [13, p. 1088]. It is therefore no surprise that many roboticists take inspiration from nature to design their systems. For example, insects have affected many drone designs that attempted to recreate insects' efficient flying, high maneuverability, and small size [14–23]. However, maneuvering and landing small drones can be extremely challenging due to the limited sensing equipment and reduced power density that lightweight platforms have at their disposal due to weight restrictions [24, 25]. Once again, nature offers different working solutions, some of which have been recreated by researchers to varying degrees of success. One particular biological phenomenon that has fascinated first biologists, and more recently aerodynamicists and engineers, is the dispersal mechanism of samaras, also known as maple seeds, which enter a state of passive autorotation that significantly reduces their falling speed.

In many of these papers, strong parallels are drawn to the flight dynamics of helicopters, and similar terminology is used. Throughout this section, the axis definition of the samara that will be used will be the same as shown in Figure 1.1.

Samara and Classical Aerodynamics

Norberg [1], in 1973, was the first to conduct a stability analysis of the flight of single-bladed samaras. The author performed a qualitative analysis of the stability along the pitch (feather) plane, the coning (flapping) plane, and tip path plane (related to directional stability). Norberg identified the interplay between aerodynamic, gravitational, and centrifugal forces, and attributed static pitch stability to a movement of the center of pressure around the center of mass as the angle of attack changes, creating a restoring moment. The importance of the role of center of pressure movement for the stability would later be put into question by other researchers, who stated that while this phenomenon contributes to the stability, it is not the only reason, nor is it the most significant [26]. Dynamic stability in pitch is instead two-fold, the short-period oscillations being damped in the same manner as previously described by the changing angle of attack, while the long-period oscillations are damped by a change in rotational and sinking speed during a revolution. In Norberg's paper, the samara was assumed to be analogous to a flat plate in a straight glide, with the vertical component of the centrifugal force acting together with the gravitational force. As the glide path increases beyond the

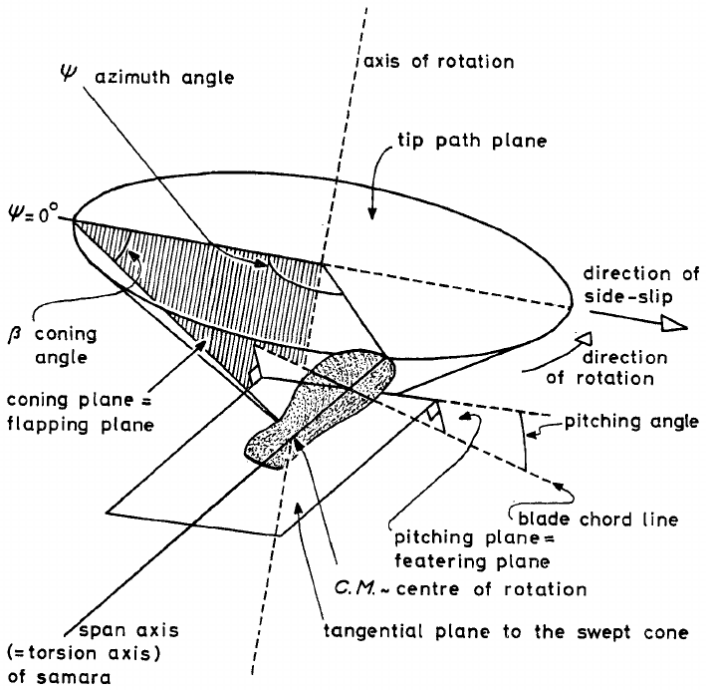

Figure 1.1: Diagram of the samara planes and axis [1].

natural angle, there is a nose-down movement of the blade that maintains the angle of attack constant, which points the resultant aerodynamic force forward. This creates a propulsive component that speeds up the rotation, and due to an increase in horizontal flow there is a restoring nose up movement, which is again caused by the attempt to maintain a constant angle of attack. This tendency towards the natural gliding angle of the samara was also shown to be interrelated with the overall descent speed. As the pitch angle changes, the resultant aerodynamic force will not be equal to the weight, and, in a similar method as for pitch stability, the blade eventually settles in the natural gliding path angle [1]. For the coning angle, Norberg stated that stability is achieved due to the interplay between the aerodynamic and centrifugal forces. If the rotation speed increases, the lift over the blade also increases, causing a positive roll moment that increases the coning angle. At the same time, an increase in rotation speed

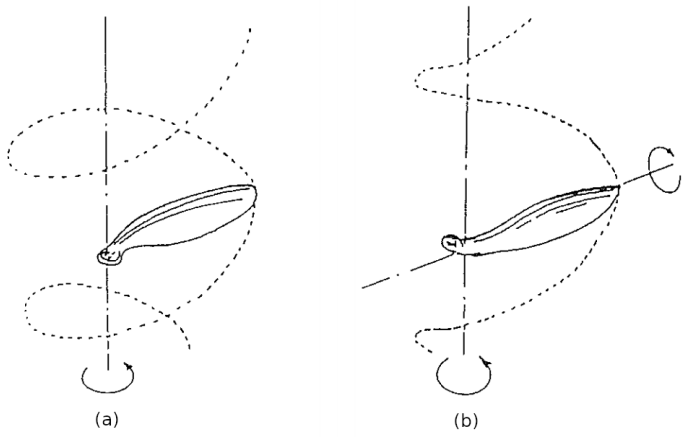

Figure 1.2: (a) Rotation about spin axis (b) Rotation about feather axis [2].

and coning angle will also increase the centrifugal force, which causes a negative roll moment that reduces the coning angle, leading to stability in this plane [1]. Finally, with regards to the tip path plane, a tilt in a certain direction will cause side-slip in the direction of the low side. Side slip has different effects that depend on the azimuth angle of the blade, increasing the resultant velocity as the blade advances in the direction of the side slip, and decreasing it when retreating. As the velocity changes, the angle of attack will also change, and, as explained previously, this will lead to a variation in pitch during the rotation. However, as the samara behaves like a gyroscope, the maximum aerodynamic force the blade will experience will be 90° after azimuth angle corresponding to the maximum resultant velocity, leading to a restoring moment that carries the tip path plane back towards the horizontal (ground) plane [1].

Interested by the autorotation and mechanics of samara, a number of researchers investigated the performance and geometric properties of maple seeds against other types of seeds. McCutchen [27] compared free-falling ash and tulip seeds with samara, conducting an experiment with ballasted seeds made from file cards to measure the different sinking speeds. The author noted that ash and tulip trees not only spin like samara, but also rotate about their feather axis, illustrated in Figure 1.2. While ash and tulip seeds fell faster than maple seeds, they were more stable, suggesting that the windier climate they developed in caused them to develop a dispersal method that was more resistant to disturbances caused by turbulence and wind gusts [27]. Lugt [28] studied autorotation itself from an aerodynamics perspective, explaining experimental observations with potential flow theory. The author noted that thicker and cylindrical plates demonstrated lower rotation (or no autorotation at all) compared to thinner plates, but fell short of explaining the coupling of inertial and aerodynamic forces due to the challenges of gathering data of autorotating bodies [28]. Azuma and Yasuda [29] extended the analysis of Norberg [1] by applying simple momentum and blade element theory. Again, difficulties were encountered in obtaining data on the lift and drag coefficients due to the complex geometry of the seeds, and the low Reynolds number in which they operate. Using a vertical wind tunnel, they collected a large amount of data on the autorotation of ten species of real seeds, suggesting that a similar method could be used to determine the aerodynamic characteristics of insect wings. Applying the local circulation method, the authors conclude that the most of the autorotation driving torque is generated at the mid-point of the seed blade, while the lifting force is highest at the tip [29]. In a later paper, Yasuda and Azuma suggested that to guarantee autorotational flight, the wing camber and surface roughness, including the leading edge, were the most significant factors [30].

Seter and Rosen [2, 26] modified the blade element method to increase its applicability to the samara, which experience much higher coning angle and angle of attack compared to helicopters, as well as significant spanwise flow [2]. Their numerical model attempted to study the effect of physical parameters on the stability of the motion, finding a high sensitivity with the chordwise mass distribution of the samara, and that, while an increase in mass resulted in an increase in the sinking rate, the highly nonlinear coupling between the different parameters made it very difficult to single out an individual parameter responsible for determining the rotational speed. The authours therefore suggested that a complete, coupled six degree of freedom model would be needed to draw significant conclusions in this matter [26]. Ulrich and Pines [31], in an attempt to investigate the best planform geometry for lowest descent speed of a mechanical samara, noted that, unlike suggested by Seter and Rosen [26], even during steady vertical descent the roll and pitch do not remain constant nor small, an assumption that is crucial when setting the trim state around zero roll and pitch. They relate wing geometry to lift generation based on theoretical and empirical data that assumes conventional attached flow aerodynamics, but this assumption is not applicable to the aerodynamics of insects and auto-

rotating seeds like samaras, which experience angles of attack up to 90° at the root [32]. Large discrepancies were always present between model predictive forces and measured instantaneous lift forces, with lackluster explanations for the cause of the higher than expected lift in both samara and insect flight, until Ellington et al. [33] published a paper that showed proof of the presence of a leading edge vortex (LEV) over hawkmoth wings, which could explain the augmented lift forces. The LEV observed was compared to those seen over swept delta wings, although generated by a very different mechanism. The authors attributed the formation of the LEV to the strong spanwise flow, which prevented the LEV from growing to the point of bursting. The researchers also noted that while there is proof that spanwise flow affected the stall characteristics of helicopters and wind turbines, no LEVs had been observed even though the centrifugal accelerations are significant, and they hypothesized that this could be due to the much higher Reynolds number, or the high aspect ratio characteristic of helicopter blades [33]. A few years later Lentink et al. [34] were also able to show the presence of a LEV in autorotating seeds flying at Re 1000.

Samara and Unsteady Aerodynamics

With the knowledge of the existence of leading edge vortices, the research shifted from a biological perspective, which aimed at correlating physical properties to the flight dynamics, to more of an aerodynamic perspective, which attempted instead to find the cause of the generation and stability of the LEV and its contribution to the lift. As the LEV appears in both the autorotation of the samara and the flight of insects, insight can be gained even from papers that do not discuss autorotating devices (natural or artificial). Revolving wings are used in many experiments that study the steady aerodynamics components of insect flapping motion, like spanwise flow and induced velocity caused by tip vortices [3].

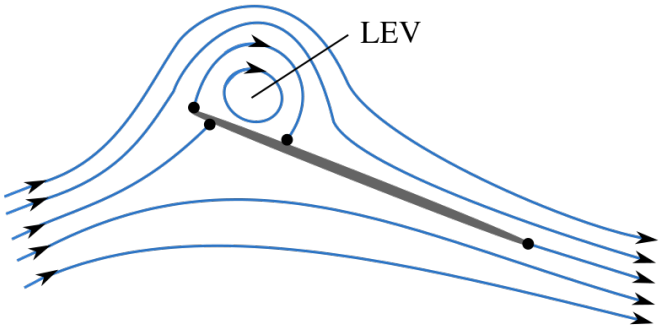

Figure 1.3: Illustration of leading edge vortex [3].

While LEVs were confirmed as the method through which higher than expected lift forces were generated, there is still debate as to the condition under which the LEVs are created, and the mechanism by which they remain stable. The first hypothesis with regards to the samara was made by Lentink et al. [34], who stated that the LEV remains stable partly due to a similar phenomenon as observed in delta wings, where the spanwise flow drains the vortex's vorticity and prevents it from growing to an unsustainable size that leads to separation [34]. In the same paper, the authors noted that the aerodynamic efficiency increased with decreasing angle of attack, as the LEV becomes more compact. Birch and Dickinson disproved this spanwise flow hypothesis by conducting experiments where edge baffles and fences were used to block the spanwise flow, and showed that the LEV remained attached regardless [35]. Limacher and Rival [36, 37], who studied the topology of the flow over the samara, supported these findings,

and found that tip speed ratio was a key driver for the flow behavior, but not for the leading-edge circulation. Increasing tip speed ratio results in a stretching of the leading edge vorticity, causing the LEV to become more compact [36], but has negligible effect on the effective angle of attack and induced velocities [37].

In a follow-up study, Lentink and Dickinson [38] combined theoretical predictions of boundary layers of spinning disks and experimental results, and further investigated what factors play a role in the LEV stability. First, they varied wing sweep to check if this property alone could stabilize the LEV, and found that, unlike highly swept delta wings, increasing sweep both increased vortex shedding and decreased lift generation for Re 110 to 1400. They then investigated the role of angular acceleration, characterized by the dimensionless stroke amplitude A*, and centripetal and Coriolis accelerations, characterized by the Rossby number Ro.

$$A^* = \Phi_0 R/c \tag{1.1}$$

$$Ro = R/c \tag{1.2}$$

Where Φ_0 is the stroke amplitude in radians, R the wing length, and c the average chord length. For simplicity, R is used in the definition of the Rossby number, although the correct variable would normally be the radius of gyration R_g [38]. Their conclusions were that LEV stability and force augmentation is dependent solely on a low Ro $\mathcal{O}(1)$, and is largely unaffected by Re, with their experiments ranging from Re 110 to 14000 [38]. Evidence of LEVs for large structures such as ship propellers and wind turbines also suggest that, given a sufficiently low Ro, it should be possible to use LEV-based force augmentation for Re $> 10^4$, although the authors state that more research on the effect of airfoil shape is needed for $10^4 <$ Re $< 10^5$. Angular acceleration and Re, however, affect the spanwise flow, and while they do not contribute to stability, they play a pivotal role in mediating the LEV integrity. Lentink and Dickinson finally show that revolving insect wings use a more efficient mechanism than flapping, and suggest that MAVs may be able to take advantage of LEV-based force augmentation by designing bio-inspired designs that focus on maintaining a low Ro [38]. Limacher et al. [39] developed a simplified model to test the hypothesis of the Coriolis acceleration playing a significant role in spanwise development of the LEV in rotating samara-like plates. By assuming that the Coriolis force dominated the phenomenon, the model was able to predict the spanwise development of the LEV, and showed good agreements with both previous observations and experimental results, with inaccuracies in the plate-normal direction suspected to be caused by the tip vortex downwash [39]. Jardin and David [40] also tested the rotational accelerations hypothesis, by conducting a direct numerical simulation (DNS) study of the Navier Stokes equations where they isolated the effect of centrifugal and Coriolis accelerations. The authors found that Coriolis acceleration is the key mechanism in high lift generation and LEV attachment, while centrifugal acceleration only has a marginal impact [40].

Other researchers focused on studying the geometrical properties of samara and insect wings in order to investigate their effect on the lift generation. Usherwood and Ellington [32, 41] conducted experiments where they rotated insect wings in a propeller-like fashion, to study the effect of camber, twist, aspect ratio, and leading edge detail on the force coefficients generated, taking into account the steady leading edge vortex over the wing. They found that the force coefficients were very resilient to significant variations in camber, twist, and leading edge detail for Re 1100 to 26000 [32]. The authors state that this insensitivity is not surprising if the LEV is the cause of higher lift, as LEVs are observed for paper airplanes as well as the wings of the Concorde and Space Shuttle [41]. When analyzing the data on aspect ratio, which also had minor effects on the forces, they concluded that models that assumed two-dimensional, conventional, steady force coefficients "may be in serious error" [41, p. 1572],

for wings in the Re range of bumblebees and hawkmoths. During an investigation on the initial transition to maple seeds' helical path, Varshney et al. [42] observed that even a seed with most of its wing removed was able to enter a stable descent that followed a similar helical path as undamaged seeds, albeit with a much larger falling velocity. The authors concluded that the primary reason for the seeds entering the steady helical motion is not the aerodynamics, but rather the interplay between the initial aerodynamic torques and the rigid body dynamics, characterized by the seed's distinct principal moments of inertia and therefore the inherent rotational instability about its chord axis (which corresponds to the intermediate moment of inertia). The seed quickly enters a steady state thanks to the aerodynamic forces balancing out the centripetal force [42].

Modeling Attempts

There have been a number of studies that attempted to construct a model for the dynamic behavior of the autorotating samara. As briefly mentioned at the beginning of the section, Norberg [1], and Azuma and Yasuda [29] developed simple models based on linear momentum theory, but these models did not include 3D flow effects, and Lee and Choi [43] noted that their assumption of zero far-wake velocity violates mass conservation. Other works, like the papers by Rosen and Seter [2, 26], showcased models based on the Blade Element Method (BEM). Again, these models are unable to capture unsteady effects and the influence of the wake on the aerodynamic forces, as well as being very sensitive to the initial kinematic input parameters [44]. Some papers present findings from high fidelity models based on the Navier-Stokes equations, which, while necessary to shed light on fluid-structure interactions, are impractical for understanding parameters key to the flight performance [44]. Traub [45] derived a simple analytic expression based on the leading edge suction analogy and the actuator disk theory, which allowed separation of the axial force and vortex lift. The author applied his expression for a number of insects, and found that vortex lift made up 27-50% and 23-34% of the attached flow lift and total lift respectively [45]. Rezgui et al. developed an analytical expression based on the Polhamus model for the 2D lift coefficient that includes 3D effects. The authors combined this expression with BEM to create a lightweight model capable of predicting the flight dynamics of samara. Their model showed good agreements with experimental results, although their test apparatus did not allow the seed to rotate at its natural coning and pitch angles [46]. Lee and Choi [43] applied steady wing-vortex theory to derive a scaling law that reasonably predicts the lift forces of autorotating seeds falling at terminal velocity. The authors compared their scaling law and actuator disk theory against an unsteady 3D numerical simulation, showing that the latter is not able to predict sectional lift coefficients [43]. Zakaria et al. [44] used Unsteady Vortex Lattice Method (UVLM) to predict the aerodynamic loading over the samara wing, without including body dynamics. Their results indicate that leading edge suction plays an important part in the generation of unsteady forces, and showed that samara with a curved leading edge tends to concentrate the vertical forces near the wingtip, as opposed to a samara with a straight edge, which better distributes the force [44]. The lack of a comprehensive model highlights the challenges in understanding the flight dynamics of samara, which combines unsteady, 3D flow effects with inertial forces of a non-symmetric rigid body.

1.2. Samara-Inspired MAVs

The insights gained on the flight of samara seeds galvanized innovation of new types of MAVs that resembled the plant. While these designs often only prioritize hover and not the forward flight of the drone, these papers can provide insights on the physical characteristics and control approaches necessary to achieve a stable hover with a non-conventional multi-rotor

configuration. Early attempts to design and fly monocopters ran into a number of issues related to sensing and visualizing the drone attitude during rotation. A research team from the Embry-Riddle Aeronautical University cited difficulties with pilot control of their monocopter design, the SamarEye, caused by a lack of inertial frame reference point as well as response lag stemming from gyroscopic effects of the motion, which their controller did not account for [47]. This section explores a number of designs, successful to different degrees, which were inspired by the samara and that tried to replicate its unique flying capabilities.

Ulrich et al. presented two similarly samara-inspired MAVs of different sizes (Figure 1.4) over a number of papers [6, 48–52]. Noting that previous monocopter designs were not at all similar to the samara, the authors successfully tried to design an MAV that would exhibit the same passive stability, efficient autorotation, and low mechanical complexity [48]. The Samara-I and Samara-II showcased a single blade, with a planform similar to the samara, designed according to previous research [6, 31], attached to a supporting arm holding the motor at 90° from the span axis. The motor is raised above the chord-span plane of the wing to avoid ground impingement during takeoff and landing [6]. Their gross takeoff weight (GTOW) was 125g and 48g respectively, were able to fly for 20 and 10 minutes, and were both capable of passive autorotation in case of motor failure [48]. Ulrich et al. identified a linearized model of the heave and yaw rate dynamics of their mechanical samara using a combination of data collected by the on-board sensors, and precise attitude and altitude data measured via a Vicon visual tracking system. These models allowed the authors to derive a closed-loop feedback PID controller, of which inputs were calculated offboard and transmitted to the MAV. The controller achieved initial altitude control using the MAV's two actuators, the wing collective and brushless motor [49, 50]. Their controller showed an underdamped response to a descent command, which differed from the critically damped response to ascent commands. The authors offered two possible explanations, the first being that the controller could not deal with the force of gravity acting with and against the commands, and the second being that positive changes in collective increase both lift and drag, damping the upward heave velocity, while negative changes increase negative lift forces that contribute to the large overshoot [50]. Follow-up work was done to further improve the dynamic identification, which resulted in the development of an aerodynamic, multi-body model of the robotic samara, obtained only using flight test data supported by the Vicon tracking system [51]. Directional control of this samara-inspired MAV was also developed [52]. The authors were not able to develop a control strategy that would act at the once-per-revolution level, due to limitations of the sensor packages available at the time, but instead used the externally collected information of the Vicon system to develop a control model that took advantage of the different system's response to impulse and step inputs [52]. Impulse input allowed heave velocity control (altitude), while step inputs affected the turn radius (position), allowing for full controllability of the MAV [52].

Orsag et al. [53] designed a dual wing rotating drone, which the authors named Spincopter, forced into rotation by two motors that are also the sole means of control. Orsag et al. performed an in-depth analysis of the gyroscopic stability, showing that the faster the rotation speed the more stable the drone. However, larger rotation also increased the frequency of oscillations about the feather axis, leading to gyroscopic precession due to the different aerodynamic forces generated. The authors' solution to the issue was to increase the angle to 5° between the motor axis and the planform plane, pointing the motors slightly upwards, which stabilizes the precession [53]. To achieve a horizontal force differential needed for lateral control, the motor thrust is varied in pulses during rotation, with the resulting control approach sending square inputs to the motors. The optimum pulse width was investigated, with the most efficient result being 2π, analogous to the cyclic control of a helicopter [53]. Win et al. [54], in an attempt to reduce weight and conserve power, constructed a monocopter without

a flap, and also had a motor as the single actuator. The wing planform was inspired by the samara, with a larger surface area near the wing tip. Control of the rotating platform is also achieved with a square cyclic control, with the authors justifying the use of square signals by stating that motor control can be much faster than the large control surfaces of a helicopter [54]. The amplitude of roll and pitch commands are used to compute the amplitude of the square waves and the phase of the cyclic function. The control strategy is comprised of a PID controller for the altitude, and a cascaded controller for the position, with an inner square cyclic controller, and an outer P controller which outputs roll and pitch commands [54].

Bai and Chirarattananon [55] present another new configuration that uses two samara-shaped wings with a motor placed at the wingtips, pointing perpendicular to the wingspan in line with the plane of rotation. Their drone, weighing only 13.8 g with a maximum take-off weight of 31.6 g, is shown to produce approximately 50% more lift than conventional multi-rotor designs in an uncontrolled hover. However, no attempt is made to design a control strategy, the authors citing that extensive study of the flight dynamics is necessary and is left for future work [55].

Jung and Rezgui [56] investigated the size at which a samara-like wing stops benefiting from the augmented lift due to LEVs during autorotation. They performed a number of drop test experiments using model wings of different sizes constructed to resemble a natural samara seed. Their results showed that at 8:1 scale (wingspan of around 30cm) the model wing achieved much lower rotational speed and a significantly higher descent speed, suggesting the LEV was no longer present. The authors, however, hesitated to make definitive conclusions from these results, citing potentially confounding factors that may have caused the scaled up model to not perform as it should have [56].

A team of researchers at Lockheed Martin developed a fully autonomous monocopter, the SAMARAI, inspired by the samara [57, 58]. The first iteration of the craft consisted of a monocopter with a 30cm wingspan/radius, weighing 200g, with two actuators, a motor, and a flap. The authors achieved simultaneous translational and height control by controlling the actuators with a virtual swashplate, inspired by helicopters' mechanical counterpart. Flap directions were modulated at different rotational phase angles to control the tilt of the rotation disk to achieve desired translations, while height was controlled with "collective" commands, comprised of a combination of motor and flap actuation [57]. Successful autonomous flight was demonstrated with a flight test that included take-off, translation, hover, and landing [57]. In a second iteration of the design, the authors focused on optimizing weight and flight time. The wing shape moved away from the large wingtip camber design, opting instead for a more standard rectangular planform using a symmetrical airfoil, chosen due to lower inertial loads on the wing flap. Their development process included wind-tunnel testing to choose optimal rotor layout and chord flap design, and a combustion engine to improve range and flight time. Passive stability about the feather axis was of particular importance to the authors, as active control was prohibitive due to limitations in sensing equipment [58]. Simulation showed that stability depended almost entirely on the inertial forces, and stability was achieved so long as the inertia about the rotation axis was 1.1 times the inertia about the chord axis. Flight testing was conducted on a scaled up prototype of their design weighing 100g [58].

Low et al. at the university of Singapore developed THOR, the Transformormable HOvering Rotorcraft (Figure 1.4), with the aim of constructing a structurally efficient hybrid where all components would contribute to all flight modes [59]. With the goal of developing a structurally efficient hybrid UAV, THOR is capable of independently pitching its wings to transition between a helicopter-like rotating hovering state, and forward fixed-wing flight. In their initial design, the authors put emphasis on aligning the center of gravity with the motors and aerodynamic center, such that model calculations would be simplified and pitching moments

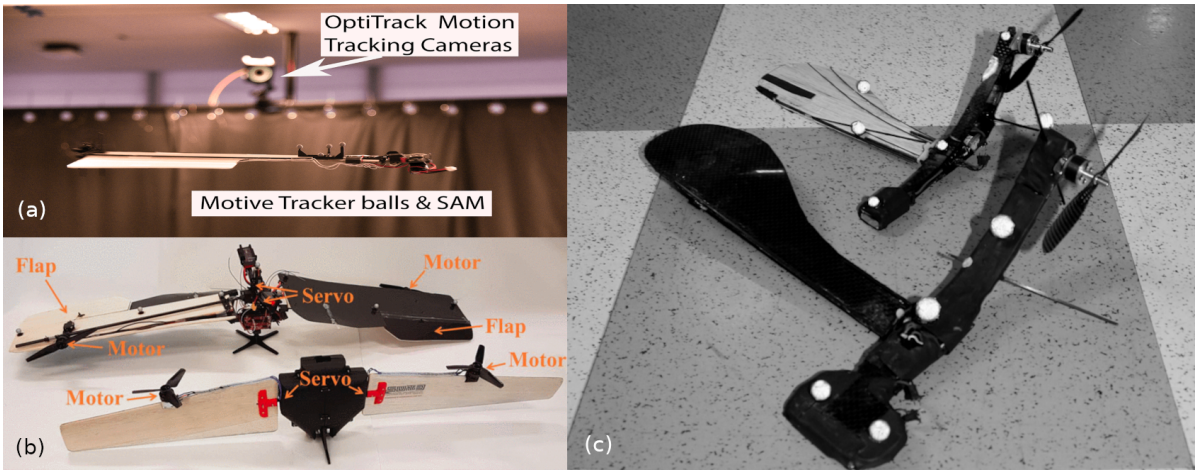

Figure 1.4: (a) SAM prototype [4] (b) THOR [5] (c) Samara-I (large) and Samara-II (small) [6].

minimized. To simulate the drone's rotation, centripetal forces and rotor-wing aerodynamics were modeled, the latter being approximated with the Blade Element Momentum Theory (BEMT). Unlike other rotating MAVs, THOR's symmetrical design allows for much more accurate results from this simplified aerodynamic theory, as the MAV behaves much closer to a helicopter [5]. After collecting data in flight tests, Low et al. apply a Fast Fourier Transform on the roll data to corroborate the IMU measurements of the drone's revolutions per second [59]. In a second iteration, Low et al. added two additional control surfaces, a flap per wing, replacing their original wing servos with centralized, higher torque, slower servos [5]. The authors justified the addition of the servos as it allowed them to mimic helicopter control by designing a virtual swashplate, with the central servos used for collective and cyclic control, as well as enabling THOR to fly in tailsitter configuration, which increases possible payload option as not all cameras can work effectively during rotation. Like for helicopters, the authors decoupled axial and forward flight by setting a fixed, optimal rotational velocity during hover mode, which greatly simplifies modeling and control design [5]. In a subsequent paper, Low et al. focused on estimating key parameters for their flight model and control of the hover mode, using a simpler, hover-only version of their MAV [60]. With the help of an Optitrack external positioning system, the authors identified aerodynamic and control parameters from experimental flight tests, taking the reader through their control solution based on helicopter control principles, but with the additional contribution of flaps and brushless motors. While prolonged fully autonomous flight still left something to be desired due to simplifications in their model, a pilot was able to easily control the drone within a 1.5m x 1.5m square space [60].

Modeling Attempts

Many papers are dedicated to the modeling attempts of monocopters and other rotating MAV platforms. Matič et al. [61] developed a mathematical model based on unsteady BEMT for the flight dynamics of a monocopter in an effort to improve model fidelity, while keeping the computational complexity low. They applied dynamic inflow theory at the blade element annulus level to avoid having to assume a certain inflow distribution over the span, allowing them to solve for the change in induced velocities directly from the thrust estimated by the blade-element and momentum theory. Different case studies were used by the authors to qualitatively assess the performance of their simplified model, and while the results agreed with the behavior of more advanced monocopter models, the simulated dynamics were not quantitatively compared to the flight test data of a real monocopter [61]. Dormiyani et al.

[62] derived a 7 DOF multibody model for monocopter free flight based on the Newton-Euler approach, using BEMT to solve for the aerodynamic forces. The model calculates the induced velocity for climb, hover, and descent separately, using vertical velocity to determine in which scenario the drone is in. This model was also only evaluated qualitatively by comparing its simulated results to the expected behavior of a monocopter [62]. Ezabadi et al. [63] attempted to identify the monocopter dynamics by using a neural network with a NARX structure (Nonlinear Autoregressive eXogenous Network), which are characterized by limited feedback coming only from the output neurons, and often used for dynamic systems [64]. The authors designed network with a single hidden layer and 15 neurons, which was unsuccessful in identifying the dynamics even when more hidden layers were added [63]. Perhaps the most successful model that has so far been developed, is the model designed by Obradovic et al. at Lockheed Martin [65]. The model is capable of full flight vehicle simulation, but relies on a multi-scale Navier-Stokes CFD approach coupled with blade-element, free-wake vortex ring models to compute the aerodynamic forces. To keep the computational complexity to a reasonable level, the 2D aerodynamic forces are computed with CFD, which are then used in a Free-Wake Vortex Lattice method to compute the 3D downwash, then coupled with BEM to approximate the aerodynamics [65].

The different monocopter models are all relatively new, but modeling rotation of larger platforms like aircraft has been a research area in aviation for much longer. Many authors have studied and attempted to provide accurate flat spin simulation models [66, 67] and upset-recovery control strategies [68, 69] for civil and military aircraft, as in-flight loss of control is one of the main source of aircraft accidents [69]. Some recent examples of simulations developed for such upset cases include the work of Malik et al. [66, 67], which developed a full 6DOF simulation with no approximations, where an aerodynamic model in the form of look-up tables was built from static and dynamic wind tunnel testing. The necessity for a high-fidelity model to accurately capture an aircraft spin motion causes these types of models to not be applicable to smaller platforms like MAVs, as the configuration and operating regimes differ greatly.

1.3. Other Rotating Platforms

While many researchers were inspired by the flight dynamics and the passively stable autorotation of samara, not all rotating platforms achieve spin by using aerodynamics, nor do they all attempt to hover, but instead merely control the position during descent. It is interesting to investigate the control strategies that allowed these unconventional platforms, not always designed with spin optimization in mind, to be able to control their degrees of freedom.

Thorne and Yim [7] attempted to design a MAV that would take advantage of the existing angular momentum of propellers to generate gyroscopic forces that could be used to control the attitude. The authors showed a theoretical advantage of their prototype, named Dysc (Figure 1.5), over traditional quadcopters with respect to agility and adaptability, and went in detail over the challenging design of their drone and the problems they encountered. In the end, experiments were conducted with a physical prototype on a gravity-compensated test stand, due to an underperformance of the main rotor, which could only generate half of the required thrust. The designed controllers demonstrated successful attitude stabilization in hover. However, no solution was offered to compensate external steady moments without saturating the gymbal joints. The authors offered additional flaps on the rotors as a potential solution, but no further development of the design was found [7].

Research of rotating MAVs does not extend only to designing new types of MAVs, but also to fault-tolerant control in case of rotor failure. Most traditional multicopters are underactuated systems, meaning that the loss of one or more rotors causes a rotation about an axis due to the unbalanced rotor torques. Mueller and D'Andrea [70, 71] derived relaxed hover solutions for

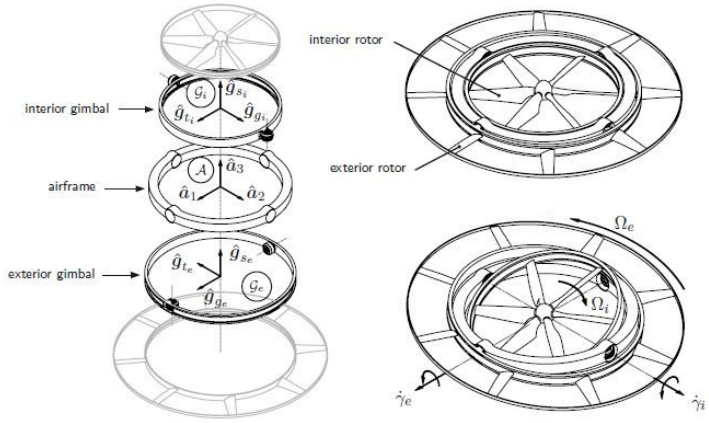

Figure 1.5: Diagrams of the Dysc prototype [7].

multicopters where the angular velocity is not constrained to zero, but must instead only remain constant. The authors demonstrated in simulation and experimental flights that by designing a controller based on these equations, a quadcopter is able to fly after complete loss of one, two, or three propellers [70]. Control was achieved with an outer position controller that assumes a damped, second-order system for the position behavior, and an inner Linear Quadratic Regulator (LQR) for attitude control, based on the linearized attitude system derived [71]. Lu and van Kampen [72] designed a control strategy that would not only allow flight of a quadcopter after the complete loss of a single rotor, but that would also be able to detect and adapt to a rotor failure, by continuously checking the estimated loss of effectiveness of each rotor against a threshold. Simulations show that the two Incremental Non-linear Dynamic Inversions (INDI) controllers, designed for both the nominal and fault-tolerant scenario, allow the quadcopter to continue tracking a given trajectory even after the loss of a propeller mid flight [72]. Sun et al. [73] noted that rotor failure is likely to occur not only near hover, but also during high speed cruising flight, and were able to design a controller that permitted a quadcopter to maintain cruising flight of up to 9 m/s after loss of a single rotor. The control strategy involves a 3 loop controller, with an outer PID position controller, a Primary Axis NDI controller that takes as input the desired acceleration to calculate the roll and pitch rates desired to control the axis or rotation (the primary axis), and finally a INDI controller for control allocation. INDI was chosen over model based approaches due to the difficulty of modeling the aerodynamic effects of rotating while traveling at significant speeds, which are instead included in the incremental form of the dynamics output equation [73].

Higashino and Nakama [74] successfully presented a novel landing method for fixed-wing UAVs that involved a flat spin. The authors made use of an "all-flying tail", in which the horizontal stabilizer of the tail was able to be deflected upward up to 90°. This control surface was essential to be able to control the pitch during the flat spin, as their particular configuration made it impossible to use the ailerons, as the lack of sweep in their wing geometry and position with respect to the center of gravity made those control surfaces ineffective for pitch control.

MAVs are not the only platform to benefit from the gyroscopic stability and aerodynamic forces generated by rotating bodies. Traditional airdrop devices like parafoils are greatly affected by weather conditions, offer low control during descent, and rely on correct packaging to avoid tangling the chute during deployment [4]. An autorotating device like the samara, on the other hand, offers gyroscopic stability that is less susceptible to weather conditions, and some degree of directional control without requiring a propulsion system [4]. With these justifications, Win et al. [4] developed an airdrop device inspired by the samara, named

Samara Autorotating Wings (SAW). The novel aspect of their design was the possibility to join multiple wings together that would collaboratively autorotate, in order to effectively fly at higher altitudes in thinner air, capable of detaching close to the ground and deliver payload to multiple locations. From simulations and experiments, a combination of 3 wings was found to provide the highest stability and lowest descent speed. The SAW offers directional control during descent, achieved with cyclic and collective control, but since no mechanical link exists between the wings, the amplitude of the control input is computed by the control software with knowledge of each wing's position relative to a reference wing [4].

In a follow-up paper, Win et al. modify the design of the SAW by integrating solar cells [75], in order to extend its service life by being able to perform data collection also after reaching the ground, for a theoretically indefinite amount of time. The addition of solar cells, however, caused certain limitations on the chord shape and flap design, which significantly impacted the performance of the controller compared to the original SAW [75].

Win et al. designed yet another airdrop device by modifying the SAW, this time replacing the flap with a small motor, and naming the design motorized SAW (mSAW) [76]. Control is achieved by varying the thrust of the motor using a square cyclic control law, with the optimal minimum and maximum square wave values found using a genetic algorithm, which the authors used to optimize the control parameters as well as the motor location [76]. The choice of square over sine waves was taken due to the former providing a "more 'punchy' response for directional control" [76, p.861].

A similar application for autorotating bodies was found by Mitchell and Marshall [77], who attempted to decrease the cost involved in cavity surveying. Traditional Cavity Monitoring Systems (CMS) are usually propped above the opening of the cavity and are not able to see past rock occlusions, as well as needing expensive equipment that raises the unit cost of such a device in the range of $100,000 or more [77]. Their idea was to take advantage of the rotation of autorotating bodies and use cheaper, single-point LIDAR to create an inexpensive, disposable device. The total cost of the authors' first prototype was $2,000, and while experiments showed that the device was able to generate point clouds from data collected during descent [77], the device failed to achieve autorotation likely due to the design of the blades, which were thin and long, similar to a helicopter, as opposed to a samara-like or pararotor designs which instead promote autorotation.

Nadal-Mora et al. dedicated a number of papers to the study of the stability, modeling, and simulation of pararotors [78–80], which are unpowered helicopter-like rotors, characterized by very low aspect ratio wings (around 1), which use the drag generated during autorotation to decelerate. Potential applications of such devices include the recovery of reentry vehicles, atmospheric data collection, and guidance and control of payload or projectiles [79]. Analytical [79] and numerical [80] simulation of the pararotor model indicated that the dynamics behavior of the device is primarily controlled by the distance between the center of mass and the rotor plane, the pitch angle of the individual blades, and the ratio of principal axis of inertia. Lowering the center of mass showed a tendency to make the pararotor less sensitive to destabilizing effects [80].

1.4. Summary

The presented literature review has shed some light on the relevant fields with regards to the project proposal. While the work done on the study of the physical properties and flight mechanics of samaras can provide insights on certain stability requirements for autorotation of single-blade platforms, the significantly different size and geometry of samaras compared to a flying-wing MAV make the approaches and results of these papers qualitative at best. However, the approaches taken and discoveries of other researchers that developed unconventional,

rotating, winged MAVs will greatly help shape the theoretical and experimental methodology of this thesis. The industry best practice when it comes to developing new UAV concepts seems to be a balance between simulation modeling and hardware testing, the former being needed to be able to quickly iterate over different potential solutions, and the latter necessary to validate the simulation, as well as bridging the reality gap in order to be able to end with a real, flyable prototype. In terms of rotor-wing aerodynamic modeling, BEM seems to be the most widely used approach, likely due to the method's simplicity while still being able to capture the fundamental dynamics of the rotating motion. Flight testing will also be necessary, and it will be important to make sure that the drone is equipped with actuators and sensors that will be able to keep up with the high rotation that a flat spin landing will induce.

2
Research Questions

As drone technology advances, their commercial application and use cases become ever more frequent. Many use cases benefit greatly from being able to perform vertical take-off and landing (VTOL), and long flight times. Current designs that fulfill these requirements include tailsitters and hybrid MAVs that combine the aerodynamic efficiency of flying wings with rotorcrafts' VTOL capabilities. However, as the MAV size decreases, the extra weight from the motors that are only used during VTOL becomes prohibitive. There is therefore a need to develop a VTOL method for small flying wing platforms, and the current proposal is to investigate a new type of landing that is inspired by the autorotating descent of maple seeds, or samara. After exploring the literature, there are plenty of examples of samara-inspired MAVs or other precision-landing vehicles that use autorotation to fly or land, but these designs make sacrifices with regards to long range forward flight, focusing on optimizing for hover, or minimizing landing speed instead.

With this in mind, the goal of the thesis is:

> *To demonstrate the viability of flat spin landing as a vertical landing method for flying-wing MAVs through the development of a control strategy that lets a pilot control the position of a flying-wing MAV in a powered flat spin by preparing an experimental setup that approximates the real flight conditions and allows for empirical exploration of the dynamics of the motion and validation of outdoor tests performed on a real flying wing MAV.*

There is no evidence in literature of a conventional flying-wing MAV being controlled during a flat spin, and therefore the primary goal of this thesis is to demonstrate the viability of this approach in order to justify and lay the groundwork for future research. Ideally, the long term end result will be a landing method that allows a flying wing MAV to reliably take off and land. To arrive at this end product there are many steps that are unfortunately not feasible within the time constraints of this thesis, and are left for future research. These future steps include being able to control not only the position of the drone, but also the descent velocity, eventually achieving hover, and then taking it a step further to be able to climb and take off.

To achieve the research goal there are a number of questions that can be asked to focus the project towards a successful result. The first requirement involves reliably entering a powered flat spin, and that while spinning the descent velocity is reduced, to show that this approach can be used as a non-destructive landing method.

1. *What combination of flight conditions and actuator inputs will allow the pilot to reliably enter a powered flat spin that can be used to land the drone?*

Investigating the initial phase of the maneuver, while not a priority in the demonstrative scope of this thesis, is nevertheless important, as being able to enter a powered flat spin reliably will allow for data to be more easily collected, and reducing the descent speed will not only confirm the landing method as a viable approach, but also allow experiments to run for a longer time to more effectively study the dynamics of the motion. These two aspects of the first research question can be further focused into the following two sub-questions:

(a) *What combination of flight conditions and actuator inputs will allow the pilot to reliably enter a powered flat spin?*

(b) *What combination of flight conditions and actuator inputs will allow the pilot to minimize the descent rate during a powered flat spin?*

In order to prove flat spin landing as a viable landing method will not only require the maneuver to show that the drone's descent can be significantly slowed down, but must also demonstrate that while spinning the drone its position can be controlled. The ability of landing MAVs vertically opens up many possibilities for operations in, for example, urban or cluttered environments, which require precision landing. The research goal therefore puts emphasis on position control of the rotating MAV, and to that end, the effect of the actuator inputs will need to be investigated.

2. *What combinations of actuator inputs will allow the pilot to control the position of a descending flying-wing MAV in a flat spin?*

From studying the current state-of-the-art, samara-inspired MAVs (almost exclusively monocopters) often implement some sort of cyclic control via a virtual swashplate. Depending on the actuators available, cyclic control is achieved by using either motors or control surfaces (elevons), both available in the MAV that will be used for this thesis. In order to develop control strategies using these actuators, it's important to know how effective these are at controlling the rotation plane, which in turn controls the position of the MAV during the flat spin.

(a) *To what extent can the motors be used to control the rotation plane?*

(b) *To what extent can the elevons be used to control the rotation plane?*

To answer these questions experiments will need to be carried out to test whether the actuators can respond quickly enough during a single rotation. Should this not be the case, better actuators will need to be installed in the MAV, or ultimately the rotations per second will need to be limited during the flat spin. This is undesirable, as lower angular velocity has been shown in literature to lead to larger descent rates. The actuator response speed will be tested for both motors and elevons, both of which can be determined with indoor bench tests.

There is a possibility that the actuators of a conventional flying wing may not be sufficient to stabilize the flat spin or generate large enough control forces such that the position of the drone can be controlled effectively. Therefore, a follow-up question can thus be asked:

3. *What additional actuators (if any) are needed by a flying-wing MAV in order to be able to control the plane of rotation during a flat-spin?*

The structure followed in literature for the development of a control strategy typically involves using a theoretical model to construct a simulation environment that allows for a better understanding of the dynamics involved and quick iteration of the strategy, followed by a validation of the simulation results by test flying the real hardware. During the preliminary phase of this thesis, unsuccessful efforts were made to develop a simulation based on the Blade Element Momentum Theory (BEMT), chosen due to its implementation simplicity and widespread use for simulation of rotating platforms, including many samara-inspired MAVs discussed in Part I. A number of key differences between simulating monocopters or conventional rotorcrafts and the flat spin of a flying wing were quickly identified, which introduced

numerous challenges discussed in more detail in Part II. Taking into account the time required to program and validate a simulation, given that the end goal involves real hardware and that the simulation should be a tool to speed up development, it was instead decided to devise a way to test the drone dynamics with a physical indoor setup.

4. *To what extent can the flight conditions be simplified in an experimental setup that yields data that can be used to quickly test control strategies and validate outdoor flight tests?*

A number of challenges need to be overcome to set up an indoor experiment representative of real flight, especially when the flight involves spinning an MAV (that cannot hover) over a prolonged period of time. It is important to think about the equipment and sensors that will be required to get meaningful data out of the experiment, and indeed *what* data allows for meaningful conclusions to be made that can then be compared to real flight test data. The research question can thus be split into the following research sub-questions:

(a) *What experimental setup allows the MAV to perform a motion representative of the real conditions?*

(b) *What experiments can be performed to produce data that can be compared with outdoor test flights?*

(c) *What equipment and sensors are needed to measure the relevant data?*

II

Scientific Article

Towards landing a deep-stalled flying-wing in a powered flat spin: a proof of concept

Matteo Barbera, Christophe de Wagter and Bart Remes

Abstract

Flying-wings show great potential for a vast number of applications, in both commercial and military sectors, thanks to their long range and fast forward flight, but suffer due to their lack of vertical take-off and landing capabilities. This paper presents a proof of concept for a novel landing method for a conventional flying wing that does not introduce additional weight dedicated only to the landing phase, with the aim of controlling a deep-stalled flying-wing in a powered flat spin. Through cyclic actuation of the servo motors and elevons, lateral forces as well as moments can be generated to control the position and attitude of the rotation plane. A successful indoor experiment was performed with a modified Parrot Disco in a controlled environment. Outdoor tests, however, failed to replicate the indoor results due to additional challenges present in the real flight conditions. A number of key challenges were identified, and the insights gained in this research lay an initial foundation for future work on this topic.

Introduction

Thanks to the miniaturization of electronics and sensing equipment, Unmanned Aerial Vehicles (UAVs) have found themselves at the forefront of robotics research, and are poised to fulfill tasks that include transportation of critical goods such as medicine, aiding disaster relief efforts, and inspection of dangerous or confined spaces that will help reduce risk to human life[1]. These applications span a wide range of industries, and each requires a vastly different drone configuration, all of which present benefits and drawbacks. The popular quadcopter design, for example, sports an agile and hover capable flight, but suffers from high power consumption[2]. Flying wings, on the other hand, showcase fast and aerodynamically efficient flight, but the traditional configuration is incapable of hover or of vertical take-off and landing (VTOL)[3].

The lack of VTOL capabilities presents a serious drawback on what is otherwise one of the longest endurance UAV platforms, as many missions envision the drones operating in urban or otherwise cluttered environments. As a result, hybrid designs have soared in popularity, combining the long flight times of flying wing with the VTOL ability of multicopters[4]. These dual systems utilize a rotocraft system dedicated only to take-off and landing, and separate motors for forward flight[5]. These types of vehicles are characterized by their low mechanical complexity and stability[5], but the addition of the rotorcraft system introduces a significant weight penalty that becomes more pronounced as the size of the drone decreases. Tilt-rotors feature a similar configuration, but are capable of rotating part of their body to point the motors in the direction of flight[4,6]. This design, while being more weight efficient, introduces control challenges during the transition phase from hover to forward flight[7] and additional mechanical complexity. Tailsitters, on the other hand, achieve VTOL by pointing their motors upward and transition to forward flight by rotating their whole frame 90°. Their flight envelope proves to be non-trivial to model, and poses a number of control challenges[8], while offering an alternative that is mechanically simpler.

Figure 1. Modified Parrot Disco. The standard pusher motor was replaced with two reversible puller motors to power the flat spin. The nose cone was added to house ballast to shift the center of gravity forward.

The inability of flying wings to land vertically is a known disadvantage of these types of conventional, lightweight, long-endurance UAVs, and a number of researchers have attempted to address this shortcoming by presenting controllers capable of landing fixed-wing and delta-wing drones while in a deep stall, showing viable results in both simulation[9,10] and outdoor flight tests[11–13]. A deep stall occurs when an aircraft's angle of attack is significantly higher than its stall angle, which results in low horizontal

velocities and large drag forces that reduce the vertical descent speed sufficiently to allow lightweight UAVs to survive the landing impact[13]. The controllers of these papers focus on trimming the drone to a stable deep stall state using elevators[13], all-moving tails[11,12], or morphing wings[10], deriving the actuator deflections from a model that approximates the aerodynamic conditions. However, during descent there is limited lateral control due to the aerodynamic control surfaces becoming ineffective while in deep stall[11], and the high touch-down speed restrict the applicability of this landing method to lightweight UAVs[12].

More unconventional designs have also been explored, like the Transformable HOvering Rotorcraft (THOR)[14–16]. This unique UAV consists of a flying wing with two puller motors placed on the leading edge of the wings, and a central actuator capable of rotating the wings along their spanwise axis to a rotationally symmetric configuration. This mechanism allows THOR to use its wings to achieve significantly higher aerodynamic efficiency during hover compared to other hybrid designs, where the aerodynamic surfaces are not only unused but often act as a hindrance to control during hover and VTOL[16]. Control of the craft during hover is achieved in a similar manner as for helicopters, with cyclic and collective control, but as a mechanical swashplate proves unfeasible due to the entire UAV rotating, THOR's swashplate is instead virtual. Collective and cyclic control is performed using the central actuator and wing flaps respectively[15].

THOR is not the first UAV to tackle the control of a rotating platform. Over the last two decades the design and control of monocopters have been the subject of research of many papers, with a recent interest in bio-inspired monocopters that attempt to reproduce the passive stability and efficient autorotation of the samara, also known as maple seed. Examples include the Samara-I and Samara-II by Ulrich et al.[17–23], the SAM and SAW by Win et al.[24–26], and the SAMARAI by Lockheed Martin researchers[27,28]. Due to the nature of these platforms, they all utilized a control strategy akin to that of a helicopter and THOR, keeping track of the UAV state by using a virtual swashplate and controlling it by means of cyclic and collective control. Attitude and altitude controllers are decoupled and fundamentally differ only with how actuators are used to achieve the desired deflections, with a number of designs performing cyclic control by modulating flap deflections with a sinusoidal wave, and others instead modulating the servo motors either with a sinusoidal or square wave.

The challenges encountered by monocopters and similar rotating UAVs are not insignificant. The lack of a mechanical swashplate makes the sensing of the wing azimuth position and rotation disc attitude difficult to estimate with only lightweight MEMS sensors, a problem that is exacerbated with increasing rotational speed[16]. Similarly, control becomes more difficult as rotational speed increases due to the fast and accurate servo actuation required. Moreover, the payload and sensors are limited to rotationally insensitive choices, or require additional software solutions to account for rotation. If these obstacles are overcome, however, the result is a hover and/or VTOL-capable UAV that shows passive stability due to the large gyroscopic forces, efficient mass utilization thanks to having no actuator dedicated to only a portion of the flight envelope, and aerodynamically efficient vertical motion by virtue of the larger aerodynamic surfaces used.

In this paper, we present a proof of concept for a new landing method for flying wing drones, where the UAV is placed in a deep stall and controlled while in a powered flat spin by means of helicopter-like control strategies, using a modified Parrot Disco shown in Figure 1. This will enable a traditional flying wing configuration to achieve a stable and aerodynamically efficient vertical landing without requiring additional hardware that would introduce weight penalties or impact the forward flight efficiency of the UAV. Unlike past attempts at deep-stall landings, the rotational velocity can provide lateral control through more effective control surfaces, and introduces the possibility of a hover-capable UAV in the long term, through future optimization of the method. The experiments showed that if the plane of rotation is kept horizontal to the ground plane it is possible to control the position of the drone through a cyclic actuation of the motors, but showing the approach in an outdoor environment proved difficult. The Methodology section describes the approach used to collect the results of this paper. In Actuator Evaluation, the tests performed to evaluate the suitability of the actuators for the control of the flying wing during a powered flat spin are discussed. Experimental Testing showcases the indoor test results where the motion was explored in a controlled environment, while in Flight Experiments the outdoor flight test results are described. Finally, the section Discussion and Recommendations explains the hypothesized causes of the differences between indoor and outdoor test results and outlines recommendations for future research on this topic.

Preliminary Flight Tests

Hardware

The experiments of this paper were conducted using a modified Parrot Disco[a] drone frame, with its conventional pusher motor replaced by two puller motors mounted on the leading edge of the two wings. The electrical components were also completely replaced, with all the new components reported in Table 1. At the heart of the drone is the mRo Pixracer autopilot board, running the Paparazzi UAV[b] autopilot software. As will be discussed in the following sections, an accurate and consistent measurement of the yaw angle throughout the spin is crucial to achieve active control during the maneuver. To achieve this, the autopilot heavily relies on the data of the PNI RM3100 magnetometer, capable of sample rates of up to 600 Hz and with an accuracy three orders of magnitude higher than the HMC5983 magnetometer included in the mRo Pixracer.

[a] https://droneshop.nl/parrot-disco-fpv-fixed-wing-drone
[b] paparazziuav.org

Component	Role
mRo Pixracer[c]	Autopilot (includes IMU + Magnetometer)
EMAX ECO II 22007 2400KV[d]	Brushless DC motors
Diatone MAMBA F40 MK2[e]	ESC
Dinogy Graphene 2200 mAh 4S[f]	LiPo battery
FrSky Xact 5100[g]	Elevon servo motors
FrSky R-XSR 2.4Ghz[h]	Radio receiver
PNI RM3100[i] 2.4Ghz	Magnetometer
Holybro 433 MHz[j]	Telemetry module
Ublox Neo-M8N[k]	GPS

Table 1. List of hardware components.

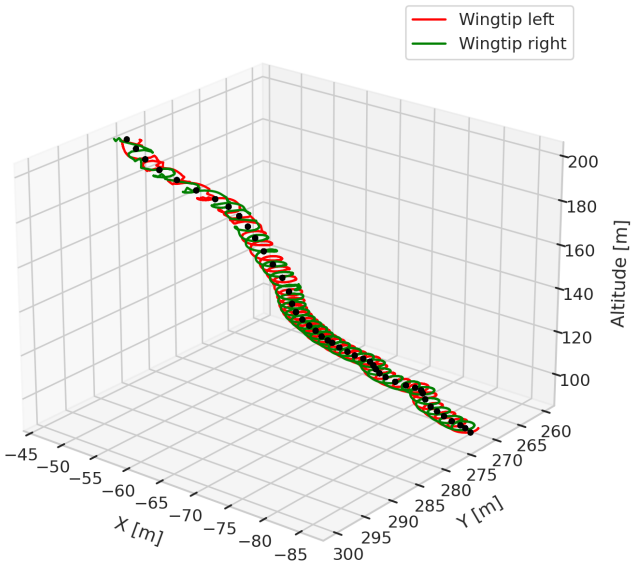

Figure 2. Evolution of drone position after initiating a powered flat spin with no cyclic thrust control, over an 11 second time interval. The path of the wingtips is approximated (not to scale). The lateral movement was caused by the wind.

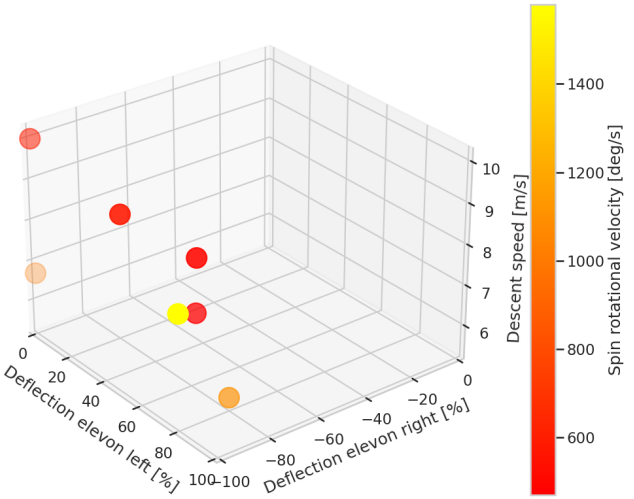

Figure 3. Combinations of static left and right elevon deflections and resulting descent speed of flat spinning drone (counter-clockwise rotation) in real flight conditions, with spin rotational velocity encoded with color. Negative deflection corresponds to a downward elevon deflection.

Minimum modifications to the aerodynamic profile of the drone were conducted, but the electronic components were completely overhauled, their replacement chosen to solve the many issues encountered throughout the development of the platform. The resulting drone has a significantly downgraded flight time, primarily due to the power hungry race-grade brushless DC motors, needed to reliably enter the powered flat spin. Future development of this proof of concept will focus, amongst other aspects, on improving the forward flight efficiency in order to work towards consolidating this approach as a viable landing method.

Powered flat spin

Preliminary flight experiments showed that it was possible to enter a flat spin by keeping the flying wing level, and then setting one of the motors to a high forward thrust setting and the second motor to a high reverse thrust setting. Figure 2 shows the drone and wingtip movement in 3D space in one such spin experiment. As the graph illustrates, the first phase of a flat spin maneuver is often characterized by a few seconds of erratic rotation before entering a more stable rotation during which the drone spins parallel to the ground plane. During this "well-behaved" spin, the flying wing experiences a high rotational velocity around the Body z axis, and the descent velocity was measured to be as low as 4-5 m/s.

Not all the flight experiments resulted in a successful flat spin where the drone spun parallel to the ground plane with a low descent velocity. It was found that certain configurations of static elevon deflections played a key role in the resulting stability of the flat spin. Figure 3 shows different elevon deflections and resulting descent speed and rotational velocity of the drone, which suggests that setting the elevons such that the drone rolls towards the rotation center leads to a higher chance of a stable flat spin. However, the data of Figure 3 is very sparse, and a more thorough investigation of the optimal elevon deflection is necessary before being able to draw definitive conclusions on the optimal static eleven deflections.

[c] docs.px4.io/v1.12/en/flight_controller/pixracer.html
[d] emaxmodel.com/products/pre-order-emax-eco-ii-series-2207-3-6s-1700kv-1900kv-2400kv-brushless-motor-for-rc-drone-fpv-racing
[e] https://www.diatone.us/products/mamba-f40-4in1-esc-mk2-dshot600-4-6s
[f] https://www.dinogylipos.com/products/2200mah-4s-70c-graphene
[g] https://www.frsky-rc.com/product/xact-hv5101/
[h] https://www.frsky-rc.com/product/r-xsr/
[i] https://www.pnicorp.com/rm3100/
[j] http://www.holybro.com/product/transceiver-telemetry-radio-v3/
[k] https://hobbyking.com/en_us/ublox-neo-m8n-gps-with-compass.html

Methodology

Theoretical Model

The dynamics of a spinning flying wing can be described on a general level by the 6DOF rigid body equations of motion in the body frame.

$$m\dot{\boldsymbol{v}} + \boldsymbol{\omega} \times m\boldsymbol{v} = \sum \boldsymbol{F} \tag{1}$$

$$\boldsymbol{I}\dot{\boldsymbol{\omega}} + \boldsymbol{\omega} \times (\boldsymbol{I}\boldsymbol{\omega}) = \sum \boldsymbol{M} \tag{2}$$

Where m is the mass of the rigid body, $\boldsymbol{v}$ and $\dot{\boldsymbol{v}}$ the velocity and acceleration respectively, $\boldsymbol{I}$ the inertia matrix of the rigid body, $\boldsymbol{\omega}$ and $\dot{\boldsymbol{\omega}}$ the rotational velocity and acceleration, and $\boldsymbol{F}$ and $\boldsymbol{M}$ the external forces and moments acting on the rigid body.

In literature, the controller design of UAVs undergoing a similar motion focuses on the estimation of the different components of the external forces and moments, which for the aerodynamic components is often achieved with the Blade Element Momentum Theory (BEMT). Trying to spin a conventional flying wing, however, introduces a number of complications that make it non-trivial to model. The approximation of the aerodynamic forces and moments of the wings and control surfaces is complicated by the retreating wing, which requires C_l and C_d data of an airfoil in reverse flow, as well as the aerodynamic behavior of a flap in reverse flow. Preliminary flight experiments also showed that the oscillations around pitch and roll during a flat spin can be as high as 30-40°, which invalidates the small angle approximation used by many BEMT models to calculate the aerodynamic forces over a blade element. The drone used in these experiments also was never able to achieve a positive climb rate or hover while spinning, meaning that the "rotor" is constantly experiencing an upward airflow between 4-10 m/s, while many models are derived while assuming the rotor is in a state of hover or positive climb. Finally, the rotational asymmetry of the UAV makes it impossible to ignore the aerodynamic and inertial coupling present in the motion. Individually, each of these issues have already been addressed in literature. There exist nonlinear BEMT models that do not make the small angle assumption[30], as well as windmill brake state models that can estimate the aerodynamic forces when the rotor is subjected to an upward airflow[31]. The Disco's C_l and C_d data could be computed from windtunnel experiments, and used together with models that augment BEMT with trailing edge flaps[32] and leading edge slats[33]. Bringing all of these elements together to address the challenges of modeling the UAV in a powered flat spin, however, is a complex task that was deemed to be geared more towards optimization rather than the demonstration of a proof of concept, which is the thesis of this paper. As such, the control strategy implemented is instead directly tested in a physical, controlled environment, to quickly demonstrate the feasibility of the approach selected and obtain empirical data that can be used to understand the challenges and work towards outdoor flights.

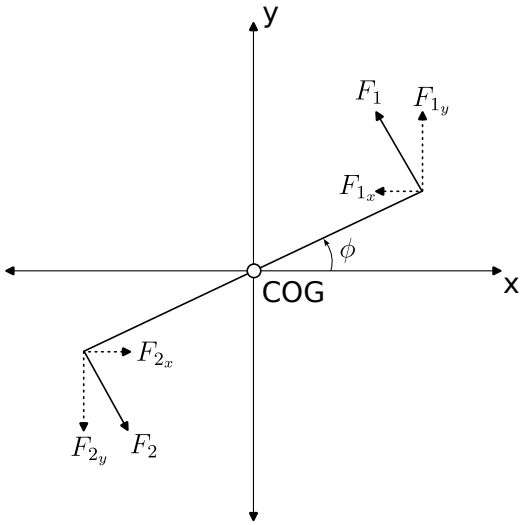

Figure 4. Simple top-down diagram of the forces generated by the motors[29].

Cyclic Thrust Control

In literature, the approach that many similar spinning rotorcrafts take to generate the lateral forces relies on approximating the dynamics through knowledge of the system. As explained in the previous section, unlike for other similar MAVs, modeling the aerodynamic conditions of a deep-stalled flat spinning Parrot Disco is a complex task. Another approach is therefore used that does not require thorough system knowledge, which aims at generating a net force disbalance over a full rotation through cyclic control of the thrust produced by the motors, inspired by the horizontal control method used by Orsag et al.[29] for their spincopter.

Using the conventions of Figure 4, the total instantaneous forces in the x and y directions at time t_0 are given by:

$$F_x = (-F_1 + F_2)\sin(\phi(t_0)) \tag{3}$$

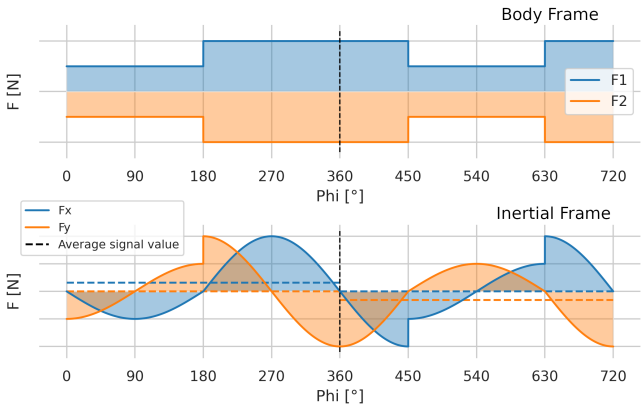

Figure 5. Top graph shows forces F1 and F2 (Figure 4) in Body Frame generated by a block signal. The bottom graph illustrates the forces along the X and Y axis of the Inertial Frame as defined in Figure 4. Integrating the average signal over one rotation yields a net force in the Inertial Frame, the direction of which can be controlled by changing the phase of the block signal. In this illustration, the phase of the block signal is increased by $90°$ after one rotation, and the direction of the net force changes from the positive X direction to the positive Y direction in the Inertial Frame.

$$F_y = (F_1 - F_2)\cos(\phi(t_0)) \tag{4}$$

To compute the largest net force that can be generated during a single rotation, define two angles $\alpha = \phi(t_1)$ and $\beta = \phi(t_2)$ such that $0° \leq \alpha < \beta \leq 360°$. The net x and y forces are given by:

$$F_{x,net} = \int_{\alpha}^{\beta} F_x(\phi)d\phi = (F_1 - F_2)[\cos\beta - \cos\alpha] \tag{5}$$

$$F_{y,net} = \int_{\alpha}^{\beta} F_y(\phi)d\phi = (F_1 - F_2)[\sin\beta - \sin\alpha] \tag{6}$$

Which show that the largest net force can be generated if $\beta - \alpha = 180°$. If $F_1 - F_2 = \Delta F$ is kept constant, the net force generated in this $180°$ interval would be canceled out in the second half of the rotation. By varying ΔF over these two $180°$ intervals, a resultant force over a full rotation can be generated, which acts in the direction of $0° \leq \gamma < 360°$, the azimuth that separates the two $[\alpha, \beta]$ intervals. In practice, a square wave command is sent to the actuators, with a period of 2π and phase angle corresponding to the desired direction of movement. This approach is illustrated and explained in detail in Figure 5.

The simplicity of this approach, which will henceforth be referred to as cyclic thrust control, allows the drone to be controlled in the x-y plane with only the knowledge of the state variable ϕ (azimuth), but has certain limitations that need to be investigated and corrected empirically. In this section's explanation no considerations were given to actuator delay and gyroscopic effects, which are expected to cause the drone to move in a direction offset from the phase angle of the cyclic control by a constant or rotational speed dependent value. Moreover, the aerodynamic forces generated by the wings and elevons are assumed to cancel each other out over a rotation, and that they will only contribute to maintaining a stable plane of rotation. In practice, the static elevon deflection required to maintain a stable powered flat spin will need to be systematically investigated in order to realize the stable conditions needed for the cyclic thrust control strategy to be used to influence the lateral position of the platform during a spin.

Cyclic Elevon Control

To achieve a higher level of controllability, the elevons can also be actively used during a spin to control the drone's plane of rotation. In literature, helicopter are able to create pitch and roll moments by means of a mechanical swashplate. Rotating UAVs make use of a "virtual" swashplate, where the aerodynamic surface deflection is computed based on an estimate of the drone's current azimuth. The same approach is used in this thesis, where a sinusoidal signal is sent to the elevons as a function of the drone's azimuth. It is important to note that due to the coupled geometry of the advancing and retreating wing, both elevons are deflected in the same direction to generate the appropriate moments, as explained in Figure 6.

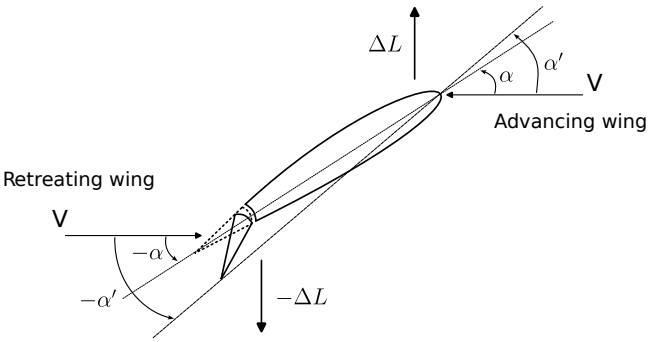

Figure 6. In helicopters, the cyclic changes the feathering of each rotor blade such that the same force is generated at the same point in the rotation. During a flat spin, however, the wings are coupled such that the retreating wing experiences a negative angle of attack. Therefore, to be able to generate the same force at a given azimuth, the elevon of the retreating wing needs to be deflected in the opposite direction as the advancing wing had been, which results in the two elevons needing to be deflected in the same direction.

Actuator Evaluation

Experimental results showed that during a powered flat spin maneuver, the flying wing experiences a rotational velocity between 1000 and 1800 deg/s. It was therefore necessary to evaluate whether the actuators could keep up with the rotational speed such that they could be used during the motion to generate sufficiently high control forces.

Elevon servo actuation speed

The elevon frequency response was computed by placing an MPU9250 IMU sensor on the trailing edge of one of the drone's elevon, and commanding the actuator to follow a chirp signal. The amplitude of the command ranged between the minimum and maximum deflection of the elevon, while the frequency was set to increase linearly over time. The rates measured by the IMU sensor were integrated to compute the maximum and minimum deflection angle achieved during each period of the chirp, and the difference between these peaks and troughs plotted against the chirp frequency in Figure 7.

Preliminary flight test showed that for a stable spin the drone achieves 1000 to 1800 degrees per second of rotation, equivalent to 3 to 5 rotations per second. In order to use this actuator for the cyclic elevon control described previously, it is necessary that it at least be able to follow two commands

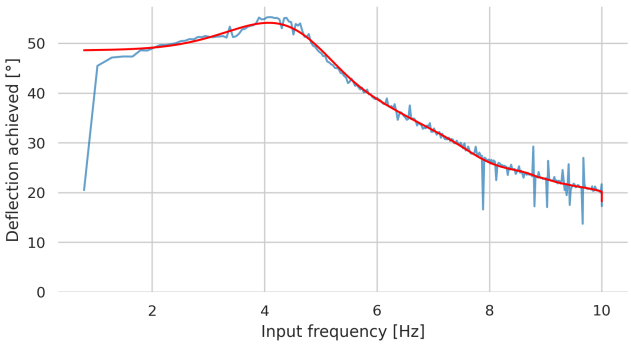

Figure 7. Elevon frequency response.

per rotation. Figure 7 shows that at 8 Hz the elevons are still capable of achieving 50% of a full deflection, which corresponds to 25°. In practice, a controller would likely not demand a full elevon deflection, as a certain static elevon deflection is necessary to counteract the aerodynamic imbalance caused by subjecting one wing to reverse flow, further confirming the FrSky Xact 5100's ability to be used for active control during a powered flat spin.

Motor servo actuation speed

Similarly as for the elevon actuators, the frequency response of the brushless motors was verified to confirm the capability of the hardware to follow the cyclic thrust control commands. Due to a lack of testing equipment rated for the high current demands of the EMAX ECO II motors, the actuation speed of of the motors was evaluated from a recording of the sound of the propellers as the motors were subjected to a sinusoidal chirp of linearly time varying frequency ranging from 0.5 to 10 Hz over a 60 second period. The spectrogram of the recording can be seen in Figure 8, which was processed to extract the highest power frequencies per time segment. The peaks and troughs of these high power frequencies correspond to the highest and lowest RPM achieved by the motor, and are shown as red and green dots respectively in Figure 9. Their difference translates to the percentage of desired command (which ranged from 10% to 100% thrust) achieved by the actuators, compared to the achieved actuation at time 0 for reference. The achieved deflection over the range of frequency of the chirp is shown in Figure 10, from which it can be seen that the EMAX ECO II motors are still capable of 50% of the desired command at 8 Hz. This demonstrates a sufficiently high frequency response of the motors, which need to work at twice the maximum rotation velocity, which, from preliminary experiments, was found to be 3-5 Hz. At 10 Hz the graph shows an unexpected increase in the gain, caused by the imperfect fitting of the peaks and troughs of Figure 9.

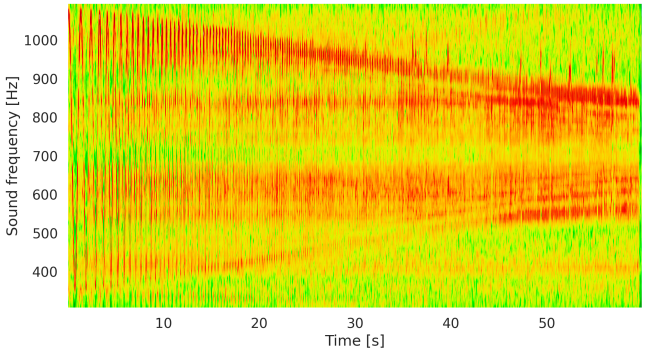

Figure 8. Spectrogram of motor sound, while subjected to a chirp of linearly increasing frequency over time.

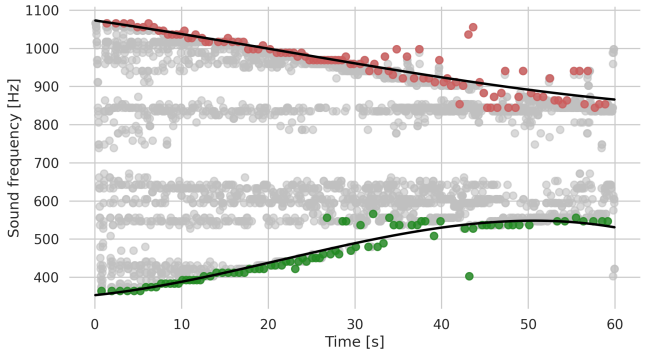

Figure 9. Highest power frequency per time segment of motor sound spectrogram, subjected to a chirp of linearly increasing frequency over time.

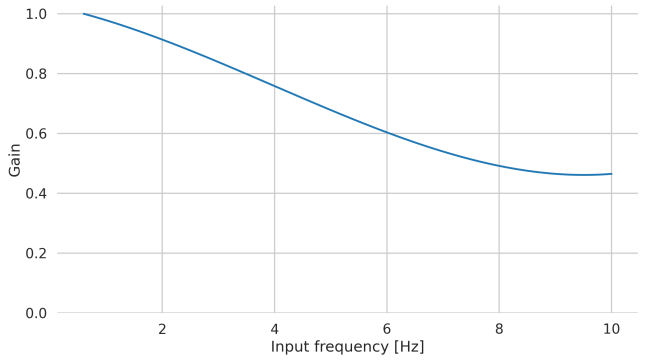

Figure 10. Motor frequency response as a fraction of the response at 1 Hz. The increase in gain at 9 Hz is caused by the imperfect fitting of Figure 9.

Reverse thrust efficiency

To power the flat spin one of the motors is set to spin in the opposite direction from forward flight, but as the propeller is not designed to generate lift in the reverse direction, a lower thrust will be generated, which needs to be accounted for to control the center of rotation along the spanwise axis. Propellers that maintain the same efficiency in both directions exist, but at the cost of forward flight efficiency, which is against the aim that this landing method hopes to achieve.

The motor-propeller thrust was measured by using the *RCBenchmark 1580*, and the linear portion of the data was fit with a linear regression to obtain the relationships between PWM and thrust generated for both forward and reverse direction, illustrated in Figure 11. Modeling the higher order behavior at low PWMs was not necessary as the powered spin requires high motor thrust settings.

After setting the PWM of the reverse motor, its linear regression equation can be used to calculate the thrust generated, which can be then used to obtain the corresponding PWM of the forward motor with the other

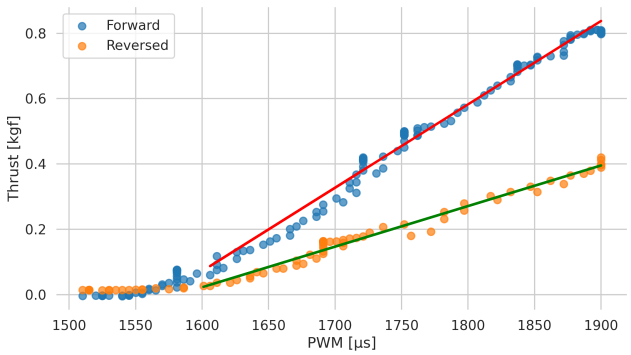

Figure 11. Difference in thrust generated between forward and reverse spin direction.

linear regression equation. In reality, the thrust generated during flight will be different than the static condition, but the approximations is sufficient to maintain the rotation center close to the desired spanwise location.

Experimental Testing

Due to the inherent challenges of trying to model a powered flat spin of a flying wing, paired with the exploratory nature of this proof-of-concept landing method research project, the bulk of the experimental testing was conducted with a constrained physical experimental setup in order to quickly understand the performance of the hardware and how to best implement the cyclic thrust control strategy.

Experimental setup

The indoor experiments were conducted within the CyberZoo facility at the TU Delft faculty of Aerospace. The CyberZoo consists of a large 10x10x7 m cage equipped with an OptiTrack camera tracking system, capable of providing pose information at up to 360 Hz. As the drone never showed hover capabilities regardless of rotational speed and elevon configuration, the flying platform was hanged from a swivel carabiner attached to the ceiling, capable of 360° rotation to allow the drone to freely spin. A high-shock high-impact fishing line was used to hang the drone, chosen due to its lightweight and low stretch characteristics for minimal interference with the tests.

Two types of harnesses were used to support the drone. The first, a 4-point harness, was initially used to investigate the cyclic thrust control strategy, as it was capable of supporting the drone while limiting excursions in roll and pitch. This permitted testing the motors in isolation, without needing to control the plane of rotation. The second harness, a 2-point harness, involved running the fishing line through the drone, and supported the craft from its belly and the whole in the canopy where the fishing line exited. Using this harness it was possible to investigate how the elevons could be used to control the plane of rotation, as the drone was able to much more freely rotate around the pitch and roll axis. A picture of the experimental setup with the second harness can be seen in Figure 12.

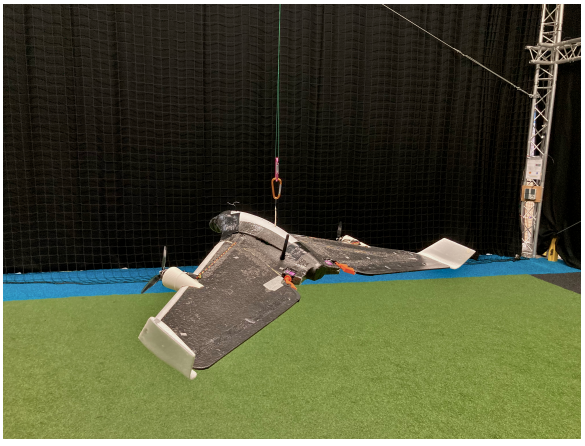

Figure 12. The CyberZoo experimental setup with the 2-point harness.

The CyberZoo experimental setup tried to mimic the outdoor conditions as accurately as possible, but still had significant limitations that need to be pointed out. Because the spinning drone is not capable of generating enough lift to hover, in outdoor conditions the platform experiences an upward flow of air ranging from 5 to 10 m/s. This has a significant impact on the aerodynamics of the motion, as the angle of attack over the wings differs greatly between the indoor and outdoor case, which prevents definitive conclusions from being drawn on the behavior of the elevons based on experiments conducted in the CyberZoo. The harness also limited the exploration of the impact that the spanwise location of the center of rotation can have on the lateral force generation and spin stability. Nonetheless, the simple and most importantly safe CyberZoo experimental setup was instrumental in understanding the key requirements for the application of the cyclic thrust control strategy in outdoor conditions.

Open loop cyclic elevon control

Cyclic elevon control was applied in the CyberZoo experimental setup, demonstrating that the elevons can be used to create moments such that the rotation plane of the drone while in a powered flat spin can be controlled. Figure 13 shows an experiment during which the spinning drone, supported by the 2-point harness, was given cyclic control commands, the phase of which was changed during the experiment with 90° degree increments. The plane of rotation in Figure 13 is illustrated by plotting the maximum roll and pitch achieved against the azimuth of rotation, with time data encoded with color. A 90° phase difference can be seen between the maximum roll and pitch achieved as would be expected for a spinning drone. The graph clearly shows the rotation plane converging to four different equilibrium states, 90° apart, corresponding to the different phase settings of the cyclic control.

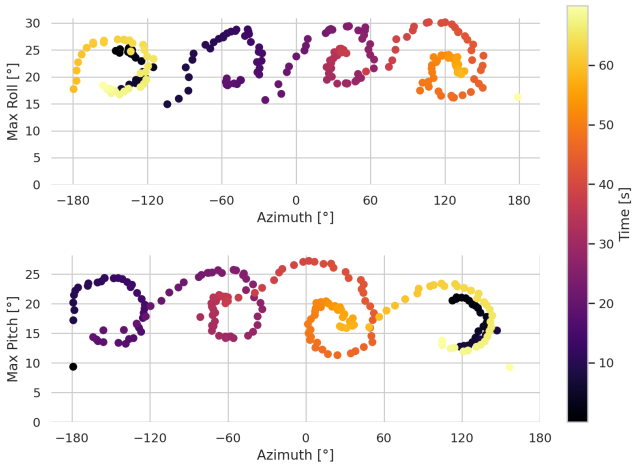

Figure 13. Maximum roll and pitch angle achieved and the azimuth of rotation at which they were achieved, to visualize the plane of rotation of the drone over time. Every data point corresponds to one rotation. The cyclic elevon control phase was changed from 0° to 90°, 180°, 270°, and back to 0° to showcase how this method can be used to create a moment and change the plane of rotation for spinning drones.

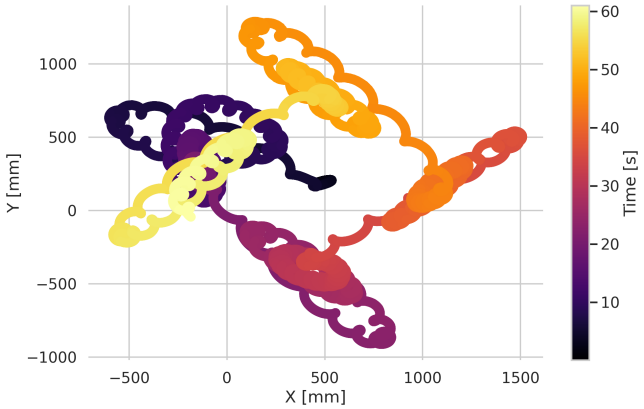

Figure 14. Horizontal position of the drone over time, with time information encoded by color. The cyclic thrust control phase was changed from 0° to 90°, 180°, 270°, and back to 0° to showcase the directional control of this method for spinning drones.

Open loop cyclic thrust control

CyberZoo experiments showed the first successful application of the cyclic thrust control strategy on this platform. The control was applied feedforward, with the phase of the cyclic sine changed at the pilot's discretion, causing the drone to move as far as the restoring forces of the pendulum setup would allow. Figure 14 illustrates the time evolution of the drone's position on the horizontal plane as tracked by the OptiTrack system, for an experimental run during which the cyclic phase was changed 4 times with 90° increments. The resulting movement shown in the graph clearly demonstrates movement in 4 perpendicular directions corresponding to the different phase settings. As the cyclic phase changed, the ensuing displacement was exaggerated by the swinging motion induced by the experimental setup, undamped due to the lack of feedback control, which resulted in visible overshoots in Figure 14, before settling to an equilibrium position.

Lateral force estimation

Using the CyberZoo experimental setup, an estimation of the lateral force that can be generated using cyclic thrust control was carried out. This was achieved by taking advantage of the geometry of the setup, which, thanks to the inability of the drone to hover while spinning, could be treated as a simple pendulum. By measuring the lateral displacement of the "pendulum" and the length of the rope from the CyberZoo's ceiling to the center of gravity of the drone, the lateral force can be estimated using the following equation:

$$F_{lat} = W \sin(\arctan(\frac{d}{l_r})) \tag{7}$$

With the lateral force F_{lat} [N], W [N] the weight of the drone, d [m] the lateral displacement, and l_r [m] the rope length. Four different cyclic thrust settings were tested, which varied the amount of thrust dedicated to spinning the drone (the cyclic average) versus force generation (the cyclic amplitude), in order to investigate the optimum settings for maximum force generation and highest rotational speed. Maintaining a high rotational speed is important to generate large inertial forces to increase spin stability. Figure 15 shows the lateral displacement of the spinning drone from its starting position in the CyberZoo over time, while Figure 16 shows the median of the displacement calculated from Figure 15 for the four cyclic thrust settings. These displacement values were used together with Equation (7) to compute an estimate of the lateral force generated, reported in Table 2. Figure 16 and Table 2 indicate that increasing the cyclic amplitude beyond $\pm 30\%$ yields too small an increase in the lateral force when taking into account the decrease in rotational speed.

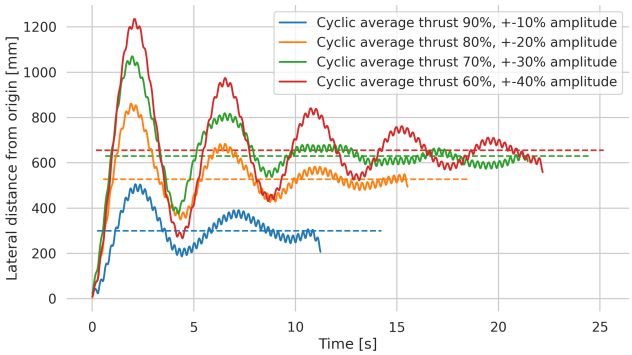

Figure 15. Lateral displacement for different motor cyclic settings over time.

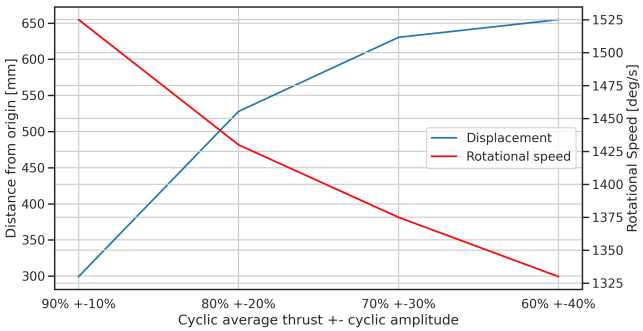

Figure 16. Lateral displacement and rotational speed for different motor cyclic settings.

Cyclic setting	Lateral displacement [m]	Force [N]
$90\% \pm 10\%$	0.299	0.623
$80\% \pm 20\%$	0.528	1.09
$70\% \pm 30\%$	0.630	1.30
$60\% \pm 40\%$	0.655	1.35

Table 2. Lateral displacement and lateral force generated by different cyclic thrust settings.

Open loop cyclic elevon and thrust control

Both cyclic thrust and cyclic elevon control can be used simultaneously, resulting in a greater degree of control for the position of the drone during a powered flat spin. Figure 17 shows an experimental run where the drone, after being placed in a spin with no active control, enables first cyclic thrust control, causing a position shift to the right, and then enables cyclic elevon control with four different phase settings 90° apart, causing an additional shift in position in four perpendicular directions corresponding to the different

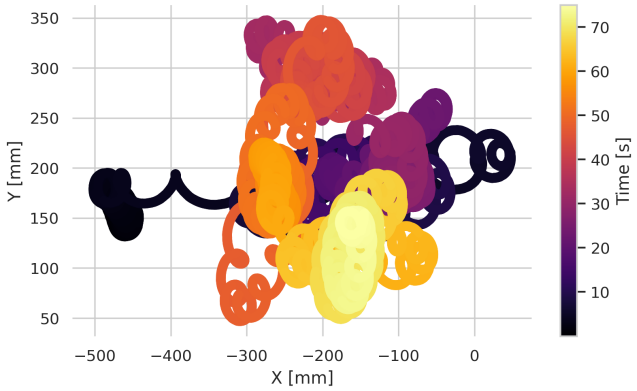

Figure 17. Horizontal position of the drone over time, with time information encoded by color. The cyclic thrust control phase was set tp $0°$, and the cyclic elevon control phase was then changed from $0°$ to $90°$, $180°$, $270°$, and back to $0°$ to showcase the additional directional control provided by using cyclic elevon control together with cyclic thrust control.

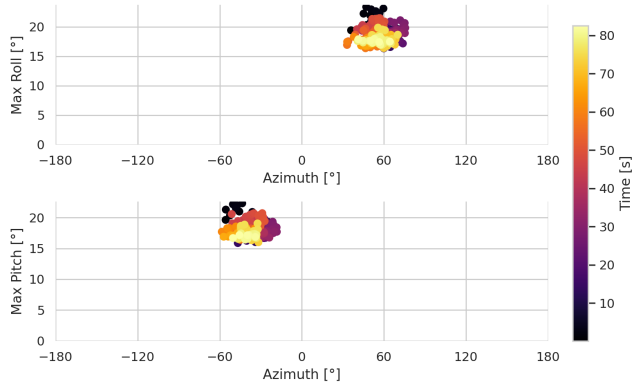

Figure 18. Maximum roll and pitch angle achieved and the azimuth of rotation at which they were achieved, to visualize the plane of rotation of the drone over time, for the experimental run shown in Figure 17. Every data point corresponds to one rotation. While using cyclic elevon control together with cyclic thrust control allowed for further control of the position of the drone, this was achieved without significant changes in the plane of rotation of the drone.

phase settings. Interestingly, however, for this experiment there is only a small change in the plane of rotation of the drone (Figure 18) compared to what had been observed in Figure 13, after the cyclic elevon control is activated. It is possible that the cyclic elevon control temporarily shifted the plane of rotation sufficiently each rotation to redirect the net lateral force generated by the cyclic thrust control, without causing a higher roll or pitch angle.

Flight Tests

A number of flight tests were conducted with the drone in an outdoor environment to test the effectiveness of cyclic elevon and cyclic thrust control in real flight conditions. Numerous spins were attempted, with very few experiments resulting in a stable flat spin where cyclic control could be activated. The original method of entering a powered flat spin consisted in slowing the drone down to a stall, while keeping the drone level, before setting the motors to a high forward and reverse thrust setting. The most successful experimental runs were instead had when the spin was initiated while the drone still carried some forward momentum. This likely helped maintain a horizontal plane of rotation in the first few seconds of the spin, allowing the rotational velocity to build up sufficiently for the gyroscopic forces to balance out the aerodynamic forces. Additionally, shifting the center of gravity aft, further away from the rotation center, as well as thrusting more with the motor on the advancing wing compared to the retreating wing, thus shifting the center of rotation spanwise, seemed to have a positive effect on the stability of the spin. Figure 19 shows four stable powered flat spins during which either cyclic elevon or cyclic thrust control was activated. In all four cases a decrease in the descent velocity is visible, but after enabling the cyclic control strategies no significant change in the descent path of the drone can be observed.

Discussion and Recommendations

While the application of the cyclic elevon and thrust control strategy in the outdoor flight tests was not able to demonstrate a capability of affecting the position of the drone during descent, it is difficult to draw conclusions on the effectiveness of the overall approach due to the significant challenges introduced in outdoor conditions compared to the indoor experimental testing scenario. The difficulties encountered in the initial phase of the powered flat spin maneuver, as well as being able to maintain a stable spin, suggests that a more systematic approach is necessary where each of these issues is investigated in isolation, before being able to investigate how effective the cyclic thrust and elevon control strategies are. For example, a more thorough investigation on the effect of static elevon deflection and spanwise location of rotation center on spin stability, as well as exploring how different center of gravity positions or engine thrust angle affect the maneuver, could be beneficial to reliably achieve a stable powered flat spin.

Empirically investigating how to best enter and maintain a stable powered flat spin can prove challenging, as it is difficult to isolate each different factor in real flight conditions. The experimental setup used throughout this thesis is also not suitable to investigate these aspects of the motion, as the current harness still somewhat limits rotational movement and does not allow a change in the location of the center of rotation. The lack of upward flow also creates a significant disparity in the aerodynamic conditions that the drone is subjected to between indoor and outdoor scenarios. Rather than having the drone hang on the rope, it would be interesting to devise a drop test, where the drone first initiates rotation and is then dropped from the ceiling, to more closely recreate the outdoor conditions, although the height of the CyberZoo is not sufficiently high to allow a steady state to be reached. Placing a large fan below the CyberZoo experimental setup could also be a solution to better recreate the outdoor conditions. A more drastic attempt to replicate real flight conditions would involve devising an experimental setup for a (vertical) wind tunnel experiment, with the drawback of being significantly more time consuming and costly, and perhaps best suited once the landing approach reaches a higher level of maturity.

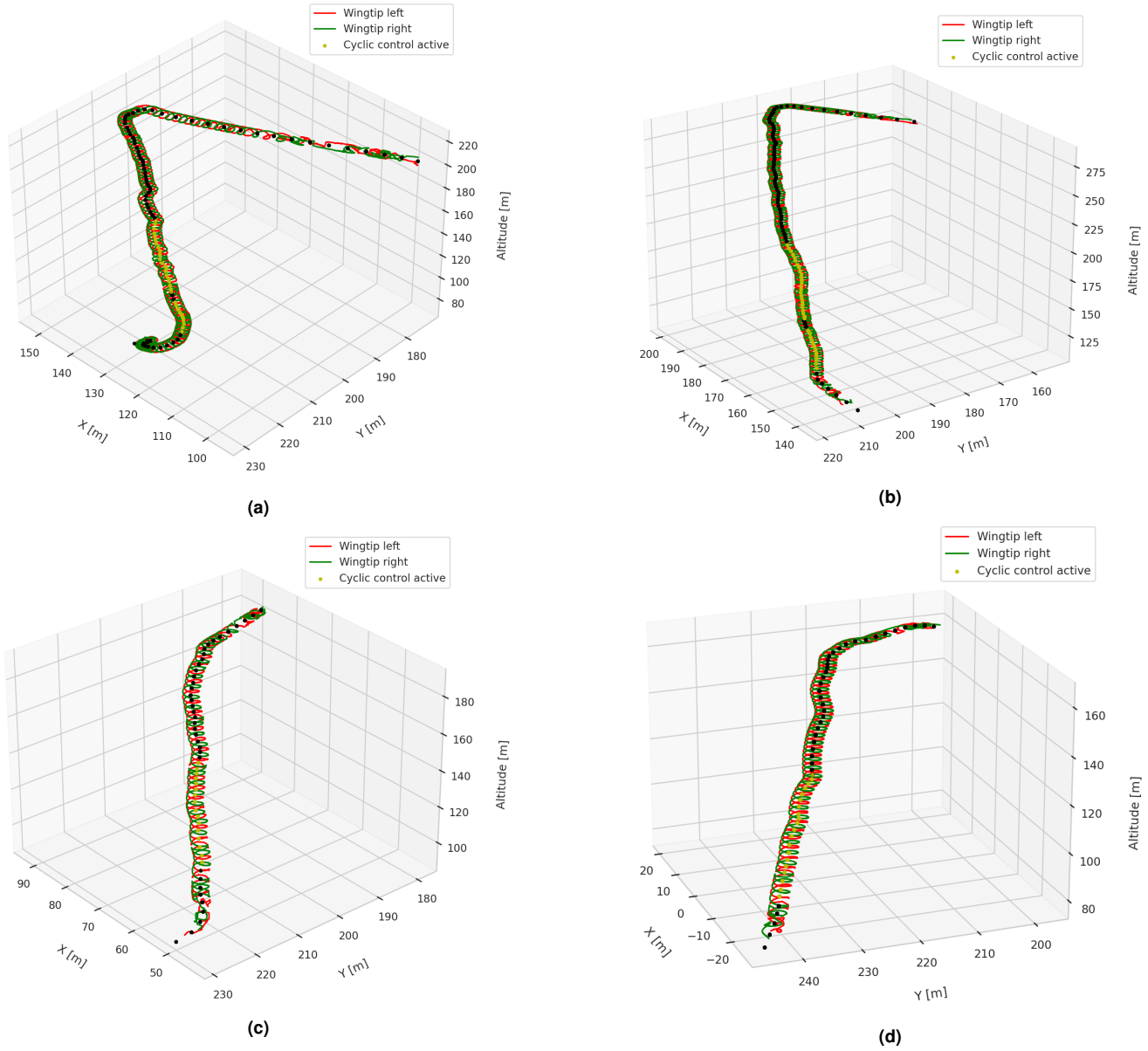

Figure 19. Evolution of drone position after initiating a powered flight spin, over a 25, 28, 13, 14 second interval for Figures 19a to 19d respectively. After the spin became stable, cyclic elevon control was activated (Figures 19a and 19b), or cyclic thrust control was activated (Figures 19c and 19d), with no clear impact on the descent path. The lateral movement was caused by the wind.

The experimental results did, however, show that entering a flat spin can significantly reduce the descent rate, and that it is possible to control the position of the drone while spinning under certain conditions. This landing approach warrants further research, and while continuing to collect empirical data could more quickly lead to a working prototype, it would be valuable in the long term to work towards a simulation environment with which the fundamental physics of the motion can be better understood. In this thesis, the challenges of creating such a simulation were better understood, and while they pushed the development of a simulation environment outside the scope of this research, its conception would prove a valuable contribution to the state-of-the-art. A simulation might also be able to provide insight on how to design a drone platform that is better suited to this type of landing than the modified Disco Parrot used in this thesis.

Many steps can be taken to better study the drone's descent while in a powered flat spin, as discussed so far in this section. The dynamics of the motion are unique, and complicated by the Disco Parrot's inability to generate large enough upward forces to be able to hover. The position of the drone was shown to be controllable as long as the plane of rotation remains sufficiently level and without the presence of an upward airflow. Another possible method of achieving control during a powered flat spin would therefore be, instead of recreating the outdoor conditions in a simulation or experimental setup, to work towards designing a flying wing that is able to achieve hover while spinning, which instead reproduces the experimental conditions in which the control strategy was shown to be working in outdoor flight. In literature, autorotating samara seeds have been shown to greatly increase lift generation thanks to stable leading edge vortices (LEVs). The conditions required for the creation and stability of LEVs are still not well studied, but the current

consensus points towards thin airfoils and low aspect ratio for revolving wings to achieve a low Rossby number between 1 and 3[34], which characterizes larger centripetal and Coriolis accelerations. Reducing the weight and size of the drone could also facilitate indoor testing, with experimental setups such as a drop test becoming more feasible.

Conclusions

By landing lightweight flying-wings in a deep stall while in a powered flat spin, their major drawback, the lack of vertical landing capabilities, can be addressed without negatively impacting the platform's endurance and aerodynamic efficiency. This paper showed a proof of concept for this landing method on a modified Parrot Disco, demonstrating in an indoor experimental setup that through cyclic actuation of servo motors and elevons control of the lateral position and attitude of the rotation plane can be achieved, with only knowledge of the drone heading and sufficiently fast servos. The same results were not replicated in real outdoor flight conditions, primarily due to a 5-10 m/s upward airflow stemming from the drone's inability to hover while flat spinning, which significantly changes the aerodynamic conditions between the outdoor and indoor experiments. Nonetheless, the flight tests showed that the descent rate can be considerably reduced after entering a flat spin. A better understanding of the system dynamics through the development of a simulation, together with modifications to the hardware geared towards further reducing the descent rate with the aim of achieving hover and climb during the flat spin can help mature this proof of concept towards a viable landing method for lightweight flying-wing drones.

References

1. Floreano D and Wood RJ. Science, technology and the future of small autonomous drones. *Nature* 2015; 521: 460–466. DOI: 10.1038/nature14542.
2. Kumar V and Micheal N. Opportunities and challenges with autonomous micro aerial vehicles. *International Journal of Robotics Research* 2012; 31(11): 1279–1291. DOI:10.1177/0278364912455954.
3. Chung P, Ma D and Shiau J. Design, manufacturing, and flight testing of an experimental flying wing uav. *Applied Sciences* 2019; 9: 3043. DOI:10.3390/app9153043.
4. Saeed AS, Younes AB, Islam S et al. A review on the platform design, dynamic modeling and control of hybrid uavs. In *International Conference on Unmanned Aircraft Systems (ICUAS)*. DOI:10.1109/ICUAS.2015.7152365.
5. López-Briones YF, Sánchez-Rivera LM and Arias-Montano A. Aerodynamic analysis for the mathematical model of a dual-system uav. In *2020 17th International Conference on Electrical Engineering, Computing Science and Automatic Control (CCE)*. DOI:10.1109/CCE50788.2020.9299157.
6. Zhong L, Yeqing H, Liying Y et al. Control techniques of tilt rotor unmanned aerial vehicle systems: A review. *Chinese Journal of Aeronautics* 2017; 30(1): 135–148. DOI:10.1016/j.cja.2016.11.001.
7. Bauersfeld L, Spannagl L, Ducard GJJ et al. Mpc flight control for a tilt-rotor vtol aircraft. *IEEE Transactions on Aerospace and Electronic Systems* 2021; 57(4): 2395–2409. DOI:10.1109/TAES.2021.3061819.
8. Verling S, Weibel B, Boosfeld M et al. Full attitude control of a vtol tailsitter uav. In *IEEE International Conference on Robotics and Automation (ICRA)*. DOI:10.1109/ICRA.2016.7487466.
9. Mathisen SH, Gryte K, Johansen T et al. Non-linear model predictive control for longitudinal and lateral guidance of a small fixed-wing uav in precision deep stall landing. In *AIAA SciTech Forum*. DOI:10.2514/6.2016-0512.
10. Zhen H, Yingying K and Da L. Deep stall landing strategy for small fixed-wing aircraft aided by morphing. In *29th Chinese Control and Decision Conference*. DOI:10.1109/CCDC.2017.7978398.
11. Park S. Control and guidance for precision deep stall landing. *Journal of Guidence, Control, and Dynamics* 2020; 43(2): 365–372. DOI:10.2514/1.G004058.
12. Taniguchi H. Analysis of deepstall landing for uav. In *26th International Congress of the Aeronautical Sciences*. DOI:10.1007/s10846-020-01264-3.
13. Pointner W, Kotsis G, Langthaler P et al. Using formal methods to verify safe deep stall landing of a mav. In *30th Digital Avionics Systems Conference*. DOI:10.1109/DASC.2011.6096086.
14. Low JE, Win LTS, Shaiful DSB et al. Design and dynamic analysis of a transformable hovering rotorcraft (thor). In *IEEE International Conference on Robotics and Automation*. DOI:10.1109/ICRA.2017.7989755.
15. Low JE, Win LTS, Lee JL et al. Towards a stable three-mode transformable hovering rotorcraft (thor). In *IEEE/ASME International Conference on Advanced Intelligent Mechatronics*. DOI:10.1109/AIM.2018.8452702.
16. Low JE, Sufiyan D, Win LTS et al. Design of a hybrid aerial robot with multi-mode structural efficiency and optimized mid-air transition. *Unmanned Systems* 2019; 7(4): 195–213. DOI:10.1142/S2301385019500067.
17. Ulrich E, Pines DJ and Gerardi S. Autonomous flight of a samara mav. In *American Helicopter Society 65th Annual Forum*.
18. Pines DJ, Humbert JS, Hubbard JE et al. Control model for robotic samara: dynamics about a coordinated helical turn. *Journal of Guidance, Control, and Dynamics* 2010; 33(6): 1921–1927. DOI:10.2514/1.50878.
19. Ulrich ER, Pines DJ and Humbert JS. From falling to flying: the path to powered flight of a robotic samara nano air vehicle. *Bioinspiration and Biomimetics* 2010; 5(4): 1–16. DOI:10.1088/1748-3182/5/4/045009.
20. Gerardi S, Ulrich E, Humbert JS et al. Hover stabilization of a controllable mechanical samara. In *AIAA Guidance, Navigation, and Control Conference*. DOI:10.2514/6.2010-7873.
21. Ulrich E, Grauer J, Pines DJ et al. Identification of a robotic samara aerodynamic/multi-body dynamic model. In *AIAA Atmospheric Flight Mechanics Conference*. DOI:10.2514/6.2010-8233.
22. Ulrich E, Humbert JS and Pines DJ. Pitch and heave control of robotic samara micro air vehicles. *Journal of Aircraft* 2010; 47(4): 1290–1299. DOI:10.2514/1.47197.
23. Ulrich ER and Pines DJ. Effects of planform geometry on mechanical samara autorotation efficiency and rotational dynamics. *Journal of the American Helicopter Society* 2012;

57(1): 1–10. DOI:10.4050/JAHS.57.012003.

24. Win LST, Win SKH, Sufiyan D et al. Achieving efficient controlled flight with a single actuator. In *IEEE/ASME International Conference on Advanced Intelligent Mechatronics*. DOI:10.1109/AIM43001.2020.9159008.
25. Win SKH, Win LST, Soh GS et al. Design modeling and control of collaborative samara autorotating wings (saw). *International Journal of Intelligent Robotics and Applications* 2019; 3: 144–157. DOI:10.1007/s41315-019-00091-6.
26. Win SKH, Goh TH, Low JE et al. Direction controlled descent of samara autorotating wings (saw) with n-wings. In *IEEE International Conference on Robotics and Automation (ICRA)*. DOI:10.1109/ICRA.2018.8463145.
27. Youngren H, Jameson S and Satterfield B. Design of the samarai monowing rotorcraft nano air vehicle. In *American Helicopter Society*. American Helicopter Society International.
28. Fregene K, Sharp D, Bolden C et al. Autonomous guidance and control of a biometric single-wing mav, 2011. Lockheed Martin Advanced Technology Laboratories.
29. Orsag M, Cesic J, Haus T et al. Spincopter wing design and flight control. *Journal of Intelligent & Robotic Systems* 2012; 70: 165–179. DOI:10.1007/s10846-012-9725-2.
30. Whitmore SA and Merrill RS. Nonlinear large angle solutions of the blade element momentum theory propeller equations. *Journal of Aircraft* 2012; 49(4): 1126–1134. DOI:10.2514/1.C031645.
31. Pratumnopharat P and Leung PS. Validation of various windmill brake state models used by blade element momentum calculation. *Renewable Energy* 2011; 36(11): 3222–3227. DOI:10.1016/j.renene.2011.03.027.
32. Yang L and Chao W. Active control for performance enhancement of electrically controlled rotor. *Chinese Journal of Aeronautics* 2015; 28(5): 1494–1502. DOI:10.1016/j.cja.2015.08.010.
33. Ravichandran K and Chopra I. Open-loop control of performance and vibratory loads using leading-edge slats. *Journal of the American Helicopter Society* 2016; 61. DOI:10.4050/JAHS.61.032003.
34. Jardin T and David L. Coriolis effect enhance lift on revolving wings. *Physical Review* 2015; 91. DOI:10.1103/PhysRevE.91.031001.

III

Additional Work

3
Hardware Optimization for Powered Flat Spin

The experiments conducted during the thesis were carried out on a modified Parrot Disco drone frame and custom electronics that greatly evolved during this research project, as different shortcomings in the hardware were identified. Many of the improvements that were made followed from experimental testing, especially when the testing resulted in a crash or malfunctioning, and certain choices that were taken speak to the inexperience of the author with hardware related issues, especially in the initial phases of the thesis project. The nature of the flat spin motion that this thesis concerns itself with truly pushes many parts of the hardware to the limit, and while the process was very challenging it was an invaluable learning experience. This chapter discusses the major challenges encountered and insights that led to the organic evolution of the hardware from its original state to the drone with which this thesis project was concluded.

3.1. Original platform and first changes

In its original state, the drone used during the thesis project consisted of a Parrot Disco, with the biggest external modification being the replacement of its standard pusher motor with two puller motors, attached to two 3D printed mounts located on the leading edge of each wing. The 3D printed mounts were irreversibly attached to the wings in a location chosen such that the mounts' surface would align with the longitudinal location of the center of gravity of the drone. The brushless DC motors used were the same as for a conventional Parrot Disco, the specifications of which are not made public by Parrot. Other than the frame, however, every other component of the drone was modified to have maximum flexibility with regards to sensors and other electrical components. The two motors connected to an mRo Pixracer board through two KISS 32A 32-bit ESCs. The Pixracer sports an STM32 Arm Cortex microcontroller, as well as an MPU9250 accelerometer, gyroscope, and magnetometer IMU combo. It also contains a separate temperature-compensated HMC5983 magnetometer, and MS5611 barometer. Connected to the Pixracer were a Holybro 433MHz telemetry module, an FrSky R-XSR 2.4GHz SBUS radio receiver, a Ublox Neo-M8N GPS, and two Parrot Disco servo motors for elevon control. The drone was powered by a Turnigy Multistar 5200mAh 3S high-voltage LiPo battery. For more detailed specifications of each individual component refer to the links reported in Table 3.1.

After some initial outdoor experimental testing of the drone platform, efforts were taken to improve the construction quality of the hardware, especially with regards to the wiring. Orig-

[1] https://docs.px4.io/v1.12/en/flight_controller/pixracer.html
[2] https://www.flyduino.net/en_US/shop/product/pr2200-kiss-esc-3-6s-32a-45a-limit-32bit-brushless-motor-ctrl-2961?category=2
[3] https://hobbyking.com/en_us/multistar-lihv-high-capacity-5200mah-3s-multi-rotor-lipo-pack.html
[4] https://www.frsky-rc.com/product/r-xsr/
[5] http://www.holybro.com/product/transceiver-telemetry-radio-v3/
[6] https://hobbyking.com/en_us/ublox-neo-m8n-gps-with-compass.html

Component	Role
mRo Pixracer[1]	Autopilot (includes IMU + Magnetometer)
Parrot Disco motors (x2)	Brushless DC motors
KISS 32A 32-bit[2]	ESC
Turnigy Multistar 5200 mAh 3S[3]	LiPo battery
FrSky R-XSR 2.4Ghz[4]	Radio receiver
Holybro 433 MHz[5]	Telemetry module
Ublox Neo-M8N[6]	GPS

Table 3.1: List of hardware components at the beginning of the research project.

Figure 3.1: Original motor wire layout.

inally, the wires that connected the brushless motors to the ESCs were taped over the wing as shown in Figure 3.1. During the first rebuild of the drone, these wires were instead braided and placed inside the wing as illustrated in Figures 3.2 and 3.3 to avoid the wires negatively affecting the aerodynamic profile of the wings.

The first rebuild of the drone was prompted by a crash that occurred during outdoor testing. Analysis of the flight logs together with the feedback from the pilot led to the conclusion that the crash was caused by the loss of RC link, resulted from the interference between the telemetry module and the radio receiver module. The location of the two was originally very close, and it was believed that the centrifugal forces experienced during the spin dislodged the telemetry module and caused it to move on top of the radio receiver, blocking it from receiving any signals. As a result, these two components were moved to be as far as physically possible as shown in Figure 3.4.

3.2. New elevon servos

Parrot discontinued its Disco models in 2018, and as such replacement components are tough to find and expensive. Therefore, the choice was made to replace all remaining Parrot components

Figure 3.2: Braided motor wire.

Figure 3.3: Improved motor wire layout, designed to restore the wing profile.

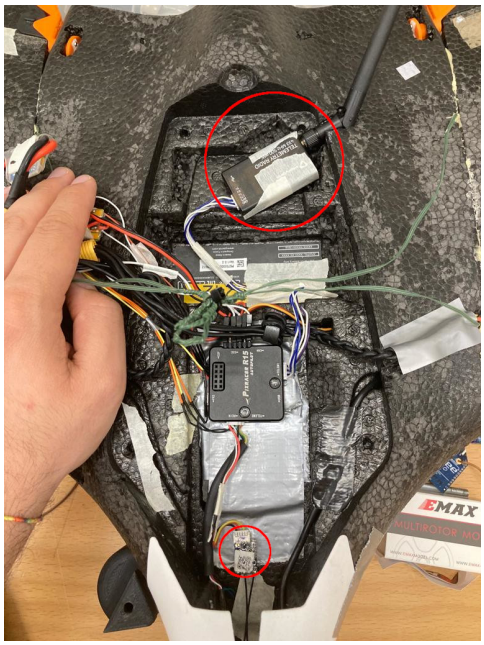

Figure 3.4: RC transmitter and telemetry module position, placed to be as far as possible to avoid interference.

with more readily available and cheaper alternatives. The elevon servo motors were one of such components that were replaced. The Emax ES08MD[7] was chosen as a replacement due to its low price and form factor. The performance on paper compared to the original servo motor was difficult to judge, due to the unavailability of specifications of the Parrot Disco servo motors. One of the unforeseen issues caused by the purchase of the Emax ES08MD was the incompatibility of its external gear with the Parrot Disco servo arm. Luckily, the Thingiverse user Hyprmtr encountered the same issue, and made available a 3D printed design[8] of a servo arm replacement, with the same design as the original servo arm with the addition of a base that allows for a servo gear (compatible with the Emax servo) to be screwed on, resulting in a solid and secure connection. Figures 3.5 and 3.6 show the produced 3D printed servo arm on its own and after the installation in the foam frame respectively. For the servo arm to move freely a small cutout had to be made to account for the larger size of the servo arm base.

[7] https://emaxmodel.com/products/emax-es08md-13g-mini-metal-digital-servo-for-rc-model
[8] https://www.thingiverse.com/thing:3287695

Figure 3.5: 3D printed servo arm.

Figure 3.6: New servo arm installed in foam frame.

Figure 3.7: Turnigy Aerodrive SK3 2826-1130kv.

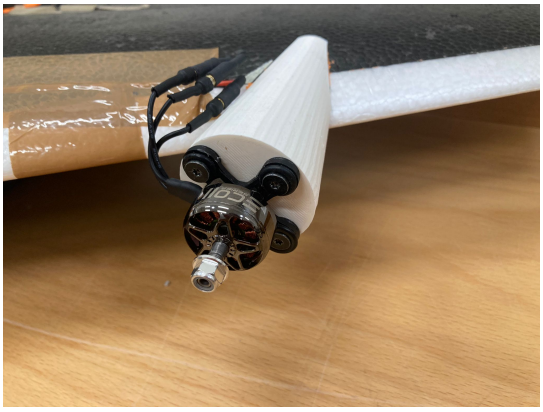

Figure 3.8: EMAX ECO II 2207-2400kv.

3.3. New brushless motors

For similar reason as for the elevon servo motors, the Disco Parrot brushless motors were replaced due to a lack of availability, price, and lack of public technical specifications. The Turnigy Aerodrive SK3 2826-1130kv[9] DC brushless motor was chosen as replacement, once again based on form factor and expected similar performance. Figure 3.7 shows the SK3 installed on the drone.

Together with these new motors a new battery was ordered, also due to the previous model being no longer available. The Turnigy Graphene 5200mAh 3S battery was chosen, with similar specifications as the previous battery although slightly heavier. Regrettably, it was discovered during an outdoor test flight that all of the hardware changes caused an increase in weight that prevented the drone from entering a powered spin. As a solution, new motors were once again ordered, this time with the requirement of being able to provide twice the maximum thrust of the Aerodrive SK3 motors while maintaining a similar form factor, to prevent lack of power from hindering any future tests. The Emax ECO II 2207-2400kv[10] motors was selected as a viable replacement, shown installed on the drone in Figure 3.8. Unfortunately, these new motors required a significantly higher current to function, making them incompatible with the ESCs and battery that were being used at the time. After testing the new motors on an RCBenchmark 1580 brushless motor test stand[11] to confirm the Emax ECO II datasheet

[9] https://hobbyking.com/en_us/turnigy-aerodrive-sk3-2826-1130kv-brushless-outrunner-motor.html
[10] https://www.unmannedtechshop.co.uk/product/emax-eco-ii-series-2207-motor/
[11] https://cdn-docs.rcbenchmark.com/wp-content/uploads/2016/01/2016-02-04-RCbenchmark-1580-datasheet.pdf

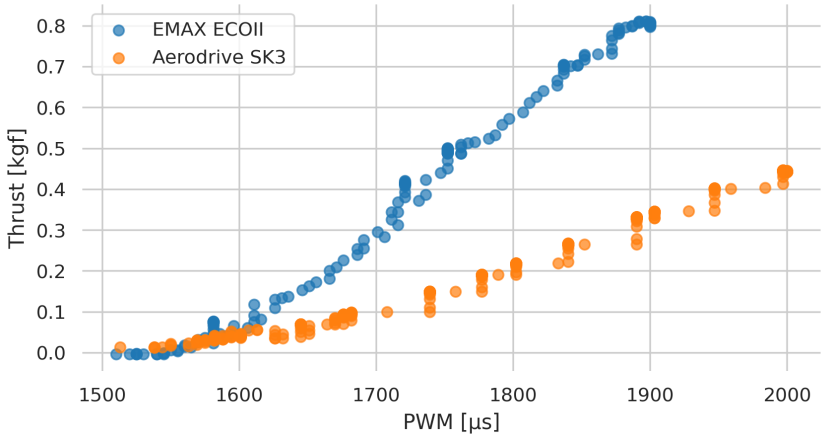

Figure 3.9: Motor thrust comparison between the Turnigy Aerodrive SK3 and EMAX ECO II motors. Due to different motor settings the ECO II maximum PWM was mapped to 1900.

values, a Diatone MAMBA F40 MK2 BLHeli_S ESC, powered by a Dinogy Graphene 2.0 - 2200mAh 14.8V 70C 4S LiPo battery was chosen to complete the powertrain of the drone. A comparison the the thrust performance of the Aerodrive SK3 and Emax ECO II is illustrated in Figure 3.9, which confirms the ability of the ECO II motors of delivering twice the thrust of the SK3 motors.

The Parrot Disco was designed to be able to detach the wings from its central body to make it easier to transport, and for the tests conducted during this thesis the wings were not only clicked together as intended by the original design, but also taped with duct tape to ensure that the wings did not separate during a powered spin. However, the significantly higher thrust produced by the new ECO II motors could produce rotational velocities so much higher than the previous motors that the resulting centripetal forces were too high for the duct tape to hold the separable wings of the Disco together. As a result, the wings had to be permanently attached to the central body part using wood glue, as shown in Figure 3.10.

The new motors were put to the test in the CyberZoo setup, in order to compare how the increased thrust performance would affect the lateral displacement that was possible to achieve within the indoor experimental setup. Figures 3.11 and 3.12 show two different experiments that were repeated using the old Aerodrive SK3 motors and the new EMAX ECO II. The impact of the new motors on force generation and lateral displacement is especially visible in Figure 3.11, where the cyclic thrust control phase was changed feedforward from 0° to 90°, 180°, 270°, and back to 0° to make the drone follow a square path.

Figure 3.10: The separable wings of the Disco Parrot had to be glued to the central body to be able to withstand the larger centripetal forces generated by the new motors.

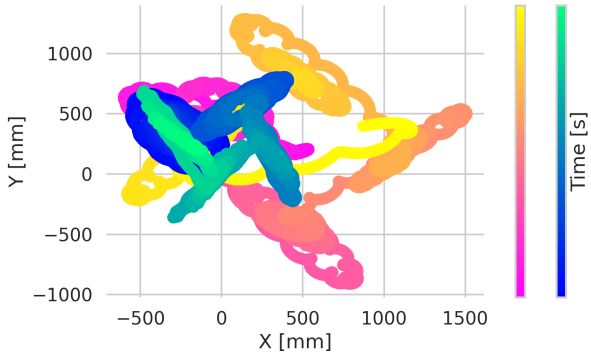

Figure 3.11: Lateral displacement, achieved during a square loop spin using two different motors, the Turnigy Aerodrive SK3 (old motors, blue) and EMAX ECOII (new motors, red).

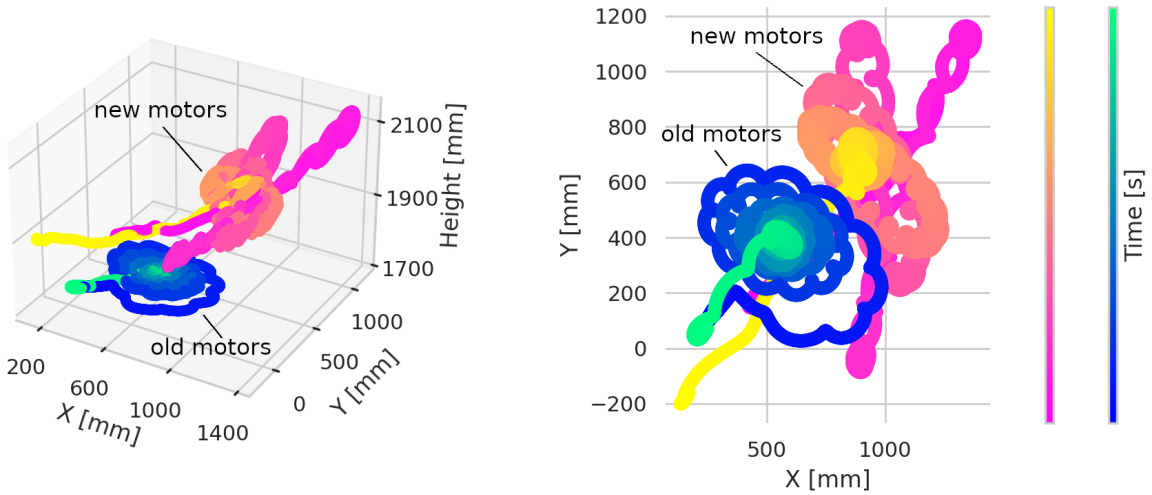

Figure 3.12: Lateral displacement achieved during a spin using two different motors, the Turnigy Aerodrive SK3 (old motors) and EMAX ECO II (new motors). Both figures show the same experiment, with a 3D view (left) and top down view (right).

3.4. Investigation of motor voltage sag

The new Emax ECO II motors were tested on an RCBenchmark 1580 brushless motor test stand[12] before integrating them with the rest of the electrical components to make sure they were compatible, and to test their performance against what was reported by the manufacturer in the datasheet. The outcome of the test results and the corresponding datasheet value is shown in Table 3.2. In terms of thrust generation, the motor performed slightly better than expected, perhaps due to minor differences in the aerodynamic characteristics of the propeller used in the two tests. As these motors were meant to address an issue related to a lack of power, the tests confirmed that the motors would make for a good replacement, but at the same time they revealed significant discrepancies with regards to energy usage that eventually required the ESC to be replaced. Table 3.2 shows a 1.9 V drop at high RPMs, and almost 3 times the current usage. The cause for this large difference was initially unknown, which triggered an extensive investigation of the ESC settings and battery in order to identify the source of the issue.

Figures 3.13 to 3.15 illustrate the performance of the battery-ESC-motor-propeller combo for different ESC settings and batteries. As these graphs show, none of these parameters had a significant impact on the voltage and current draw of the motors, with the only visible difference being an offset in the voltage graphs due to the tests being conducted on a battery at different states of charge. The investigation thus turned online, specifically to other motors with similar performance and form factor to see if they also exhibited the same issue. Indeed, the datasheet of the T-Motor Velox Veloce series[13], another brushless motor geared towards quadcopter racing, demonstrated a similar drop in voltage at maximum thrust. The conclusion of this investigation was that the large voltage sag, is characteristic of these small, very powerful racing motors, and that the cause for the discrepancy with the Emax ECO II datasheet could be attributed to the fact that for their tests, instead of using a battery, Emax employed another power source capable of maintaining a constant voltage that resulted in a lower current draw. The only way to thus reduce the effect of voltage sag would be to use a higher voltage battery (higher cell count) or a battery with lower internal resistance (higher C rating). In hindsight, the datasheet reporting a constant voltage even at maximum thrust was an indication of behavior at odds with how a battery performs under load. It was decided that since the voltage sag was, in fact, normal behavior, and since the goal of the project was a proof-of-concept rather than an optimized product that the hardware components would be left as is.

	Voltage [V]		Current [A]		Thrust [kg]	
RPM	Datasheet	Test bench	Datasheet	Test bench	Datasheet	Test bench
15700	16.8	16.3	4.7	9.5	0.30	0.31
20100	16.8	15.4	8.6	25	0.50	0.62
23600	16.8	14.7	14	38	0.70	0.79

Table 3.2: Performance comparison for Emax ECOII motors between manufacturer datasheet and RCbenchmark motor test stand. Both datasheet and RCbenchmark test were carried out using a 3-blade 5x4 propeller.

[12] https://cdn-docs.rcbenchmark.com/wp-content/uploads/2016/01/2016-02-04-RCbenchmark-1580-datasheet.pdf

[13] https://store.tmotor.com/goods.php?id=1141

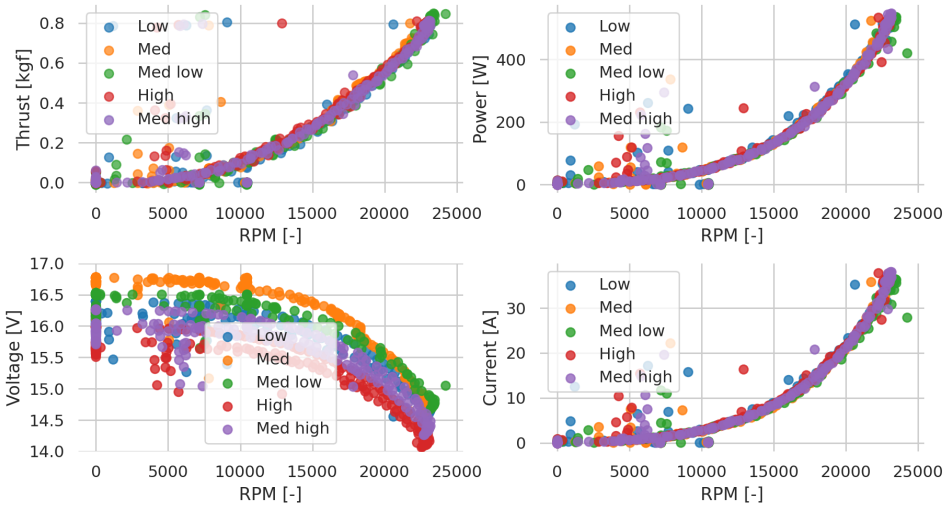

Figure 3.13: Comparison of ESC motor timing settings on motor thrust and electrical.

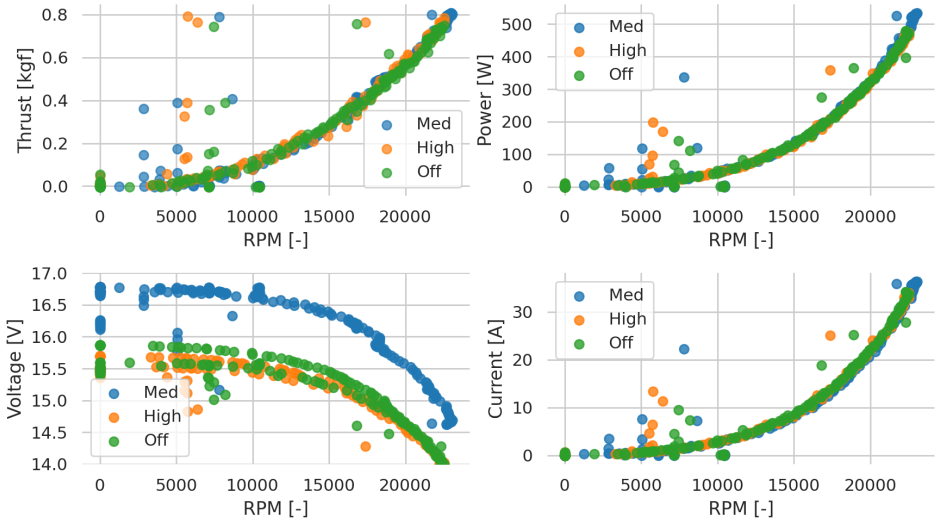

Figure 3.14: Comparison of ESC demag settings on motor thrust and electrical.

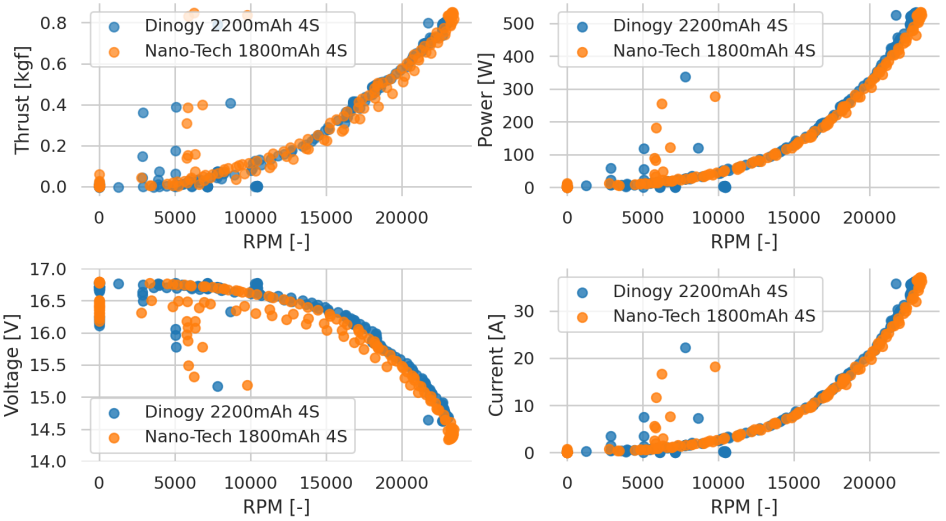

Figure 3.15: Comparison of two different batteries on motor thrust and electrical.

3.5. PNI RM3100 EXTERNAL MAGNETOMETER

Figure 3.16: Original placement of RM3100 magnetometer sensor, on the leading edge at the wing root. The proximity to the motor wire was causing interference.

Figure 3.17: Wingtip placement of RM3100 sensor, near the wingtip or the right wing. The larger distance to other electrical components improved performance.

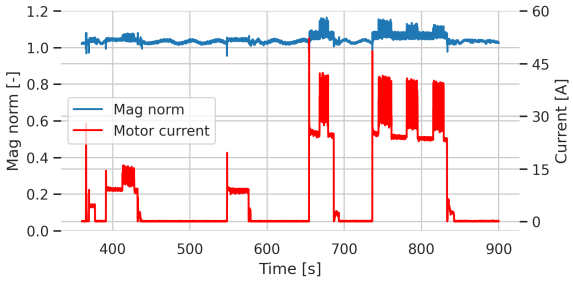

Figure 3.18: Effect of motor-generated EM field on magnetometer 3-axis norm for the original placement of the RM3100 sensor, near the motor wires.

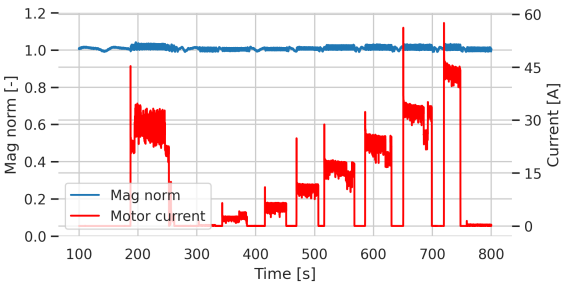

Figure 3.19: Effect of motor-generated EM field on magnetometer 3-axis norm for the wingtip placement of the RM3100 sensor.

For the proposed spin control strategy to work, an accurate high-frequency measurement of the heading is needed throughout the motion. Indoor, this is achieved thanks to the Optitrack Motion Capture System, which can provide pose information at a maximum frequency of 360Hz. Outdoor, heading estimation is achieved primarily thanks to the data produced by a magnetometer sensor, of which the Pixracer has two of, an InveSense MPU9250 3-axis magnetometer and the Honywell HMC5983 3-axis temperature compensated magnetometer. While either of them can provide satisfactory information under nominal operating conditions, they struggle to provide the high-frequency, accurate data necessary to correctly estimate the heading during the extremely high rotational velocities experienced during a spin landing.

To tackle this challenge, a PNI RM3100 military-grade high-precision 3-axis magnetometer was installed, chosen due to its maximum 600Hz sampling rate and a sensitivity 4 orders of magnitude higher than the HMC5983 sensor (13 nT compared to 0.8 mT). The sensor was originally installed near the nose of the drone as shown in Figure 3.16. There were, however, concerns regarding the sensor's proximity with the motor wire and the resulting magnetic interference caused by the high alternating current flowing through it. The RM3100 sensor was thus moved to the wingtip as shown by Figure 3.17 to test the influence of the motor wires on the sensor's performance at these two locations.

In order to test the effect of the motor current on the RM3100 magnetometer, readings at the two different locations shown in Figures 3.16 and 3.17, a flat spin landing maneuver was carried out in the CyberZoo. A magnetometer output consists of a directional vector pointing to the Earth's magnetic north, and the magnitude of the norm of its three axis should always be equal to 1. Figures 3.18 and 3.19 illustrate how the norm of the RM3100 sensor was affected by the motor current when placed near the nose and near the wingtip respectively. When placed at the wingtip, the mag norm, while still responding to high motor currents, increased by an order of magnitude lower than its original placement near the nose.

3.6. Center of gravity correction

All of the changes to the hardware caused to a different weight distribution than the original off-the-shelf platform, causing the plane to become aerodynamically unstable. For this reason a foam nose cone was designed, hollow on the inside to be able to house ballast and shift the center of gravity of the drone forward, to make it once again aerodynamically stable. The nose cone was then wrapped in tape as shown in Figure 3.20 to both attach it to the frame and to prevent the foam from crumbling.

Figure 3.20: Side view of nose cone, added to shift center of gravity forward.

3.7. New stronger elevon servos

During one of the outdoor test flights it was discovered that the Emax ES08MD elevon servos were not strong enough to be able to effectively deflect te actuator surfaces during the flight, but especially during the powered flat spin. This was attributed to a number of factors, namely servo wear and quality, as well as the stronger aerodynamic forces experienced by the wing as a result of the significantly more powerful motors. The elevon servos were thus replaced with much stronger servos, the FrSky Xact-series HV5203 metal gear servo[14]. On top of manually testing the strength of the old and new servos by pushing on the actuator surface during deflection, the actuator frequency response of the two servos was compared and shown in Figures 3.21 and 3.22. Slight dissimilarities in the servo settings resulted in different maximum deflections between the servos, as illustrated by the different deflections achieved at low input frequencies. Nevertheless, the HV5203 servos demonstrated a higher cutoff frequency and $\sim 5^\circ$ higher deflection at input frequencies higher than 6Hz when asked to perform a full actuator excursion, and deflections higher than $\sim 7^\circ$ when asked to perform half of a full excursion.

[14] https://www.mijn-hebbeding.nl/Webwinkel-Product-752567471/FrSky-Xact-serie-HV5203-8.4V-High-Voltage-High-Speed-Metal-Gear-Volledige-CNC-Coreless-Micro-Servo.html

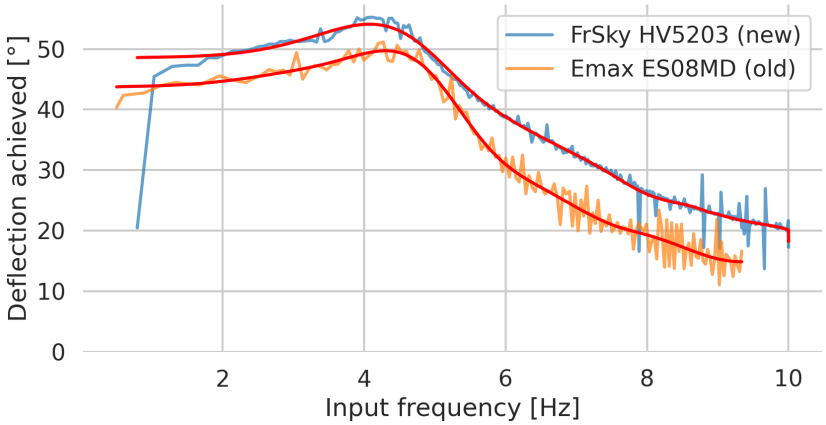

Figure 3.21: Comparison of frequency response of Emax ES08MD versus FrSky HV5203, for a deflection from full downward to full upward deflection.

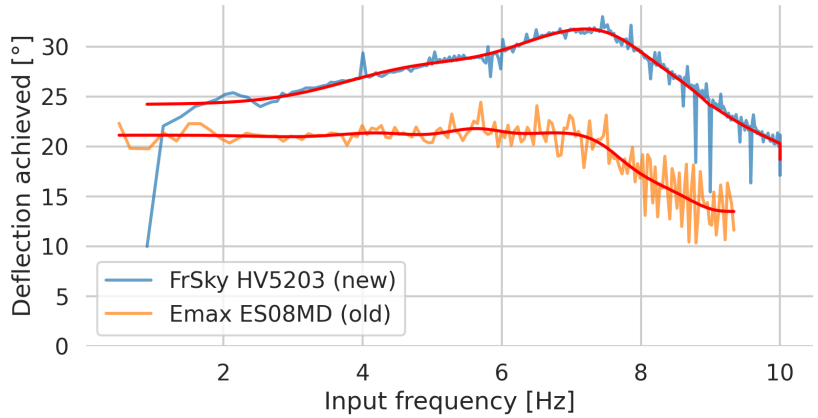

Figure 3.22: Comparison of frequency response of Emax ES08MD versus FrSky HV5203, for a deflection from neutral position to full upward deflection.

4
CyberZoo Test Flights

In order to quickly test potential strategies and to identify the challenges that would need to be solved to answer the research goal of the thesis, it was necessary to develop a safe environment where experiments could be conducted in quick succession without posing a risk to the hardware. In many of the literature works considered in the preliminary phase of the thesis research, this safe environment consists of a simulation, but certain aspects of this thesis research made it extremely difficult to create a simulation environment that would yield usable results without shifting the focus of the research from hardware to software. A physical setup was instead developed using the CyberZoo facility of the TU Delft Aerospace faculty. This Appendix chapter discusses the evolution of the CyberZoo experimental setup and the conclusions that resulted from the test flights.

4.1. Harness setup

The experimental setup consisted of the drone hanging from a rope inside the CyberZoo, with a harness holding the drone and providing a connection point to the rest of the setup. As this setup was intended to test the flat spin landing maneuver, it was necessary to have a rotating component in the experimental setup to allow the drone to rotate as freely as possible. For first iteration of the experimental setup, a swivel J-hook musket, like the ones used to hold ID cards during conventions, was used, attached to a hemp rope hanging from the ceiling of the CyberZoo, as shown in Figure 4.1. While this proved sufficient for initial tests, the design of the musket was not suitable for high rotational velocities, and the material quickly started deforming due to the motion of the drone during the experiments. As a more suitable long-term replacement, a 360° degree aluminum swivel carabiner normally used for camping was chosen. The higher quality bearing and material allowed for significantly higher rotational velocities without introducing the risk of it breaking during the experiments. Additional lightweight aluminum carabiners were used to connect the different parts of the experimental setup. These

Figure 4.1: First CyberZoo experimental setup. The drone hanged from a hemp rope, using a swivel J-hook from a name tag lanyard holder to allow the drone to rotate.

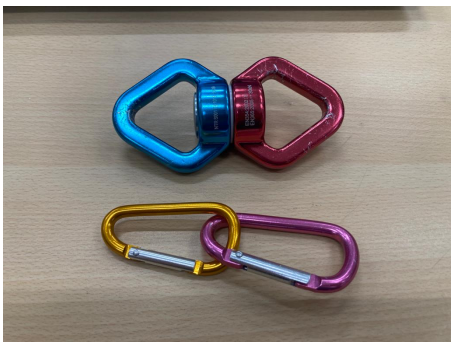

Figure 4.2: New muskets used in improved experimental setup. A 360° degree aluminum swivel carabiner was used to replace the swivel J-hook and additional lightweight carabiners were used to connect the rope to the drone harness.

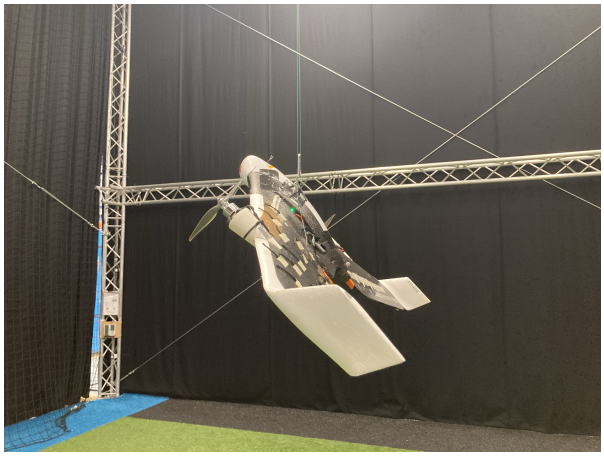

Figure 4.3: Improved CyberZoo experimental setup. A high shock and impact fishing line was used instead of hemp rope, the weight was removed, and the swivel carabiner was placed at the top of the rope to minimize interference during the spin tests caused by the weight of these components.

components are shown in Figure 4.2.

While the initial setup of Figure 4.1 had significant limitations, it allowed for a number of quick tests that helped figure out possible improvements. The main flaw of the initial setup, on top of the reliability of the rotating component, was that due to the fact that the drone was not able to generate enough lift to hover, the rope was always in tension. This resulted in the rope rotating together with the drone, and its motion had pronounced effects on the movement of the drone inside the CyberZoo. To mitigate this phenomenon, the weight appearing in Figure 4.1, was removed, the hemp rope was replaced with a high shock and impact fishing line, and the new, heavier swivel carabiner was placed at the ceiling. Important to note is the fact that a normal fishing line was not suitable for this experimental setup due to how much it would stretch under the weight of the drone. An image of the improved setup can be seen in Figure 4.3.

4.2. OptiTrack yaw ψ estimation debug

While ironing out the kinks of the experimental setup, a significant amount of time was dedicated to getting the yaw ψ to track properly during a spin. In the end, the cause of this issue turned out to be two-fold. On the hardware side, the drone was not able to receive the OptiTrack data quickly enough. This data was being communicated together with other telemetry information back and forth from the drone to the Ground Station via the Holybro 433MHz telemetry module, but because of the high rotational velocity of the spin maneuver the frequency of the OptiTrack tracking had to be set much higher than for normal operations, and the telemetry module could not keep up with all the data. To solve this, the number and size of telemetry messages being sent to and from the Ground Station was reduced, and the baud rate of the Holybro module was increased from 57600 bps to 115200 bps.

The second issue originated from how the data being received from OptiTrack was being used in the AHRS module in the Paparazzi UAV autopilot software. For the AHRS estimation, a complementary filter was utilized, which works by fusing data from different sensors by performing a weighted average with the current estimation and sensor data. The weight of each sensor's data is a static, manually tuned value that is based on the sensor's expected accuracy and sample frequency. To estimate the the yaw during normal outdoor operations, data from the gyroscope and either GPS or magnetometer is used, whereby the high frequency

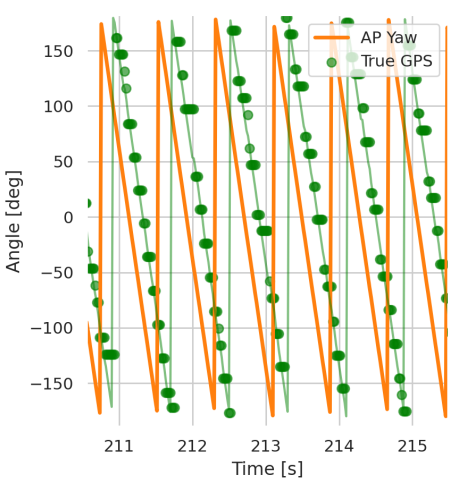

Figure 4.4: Complementary filter yaw estimate with true GPS data from OptiTrack, complementary filter set to its original correction factor.

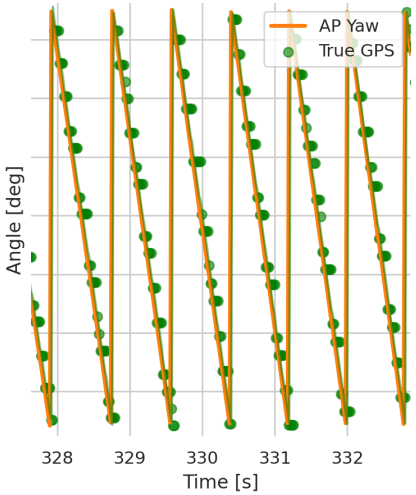

Figure 4.5: Complementary filter yaw estimate with true GPS data from OptiTrack, complementary filter set to tenfold its original correction factor.

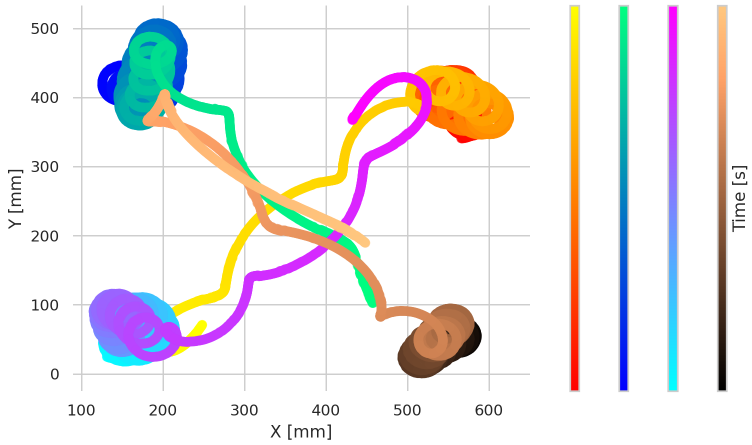

Figure 4.6: Superposition of four different experiments where the drone was asked to move in 4 perpendicular directions while spinning. The graph shows the drone movement on the horizontal plane, with time data encoded in the graph with color, the darker hues indicating the beginning of the test.

gyroscope data is integrated to provide a yaw estimate between the more accurate, albeit less frequent, GPS or magnetometer data, which also help keep the gyroscope integration error contained. In Paparazzi, OptiTrack data is used to simulate a very high frequency GPS that is much more accurate than a standard GPS module. These different sensor characteristics had to be communicated to the complementary filter through a higher GPS sensor weight, which forced the filter to trust the OptiTrack data significantly more than it would a normal GPS sensor, resulting in improved tracking of the drone's yaw during a spin. Figures 4.4 and 4.5 illustrate the improvement in yaw tracking for a higher complementary filter GPS gain.

The initial experiments revealed that for the cyclic thrust control strategy discussed in the main text of this thesis a good tracking of the yaw angle during the spin was the most important (and only) state variable necessary for the strategy to work feedforward. Figure 4.6 shows a top-down view of the drone's movement in the horizontal plane for four experiments, where the drone was asked to move in four different directions by setting the cyclic thrust phase to 0°, 90°, 180°, and 270°. The graph shows the drone being able to consistently move in the

desired direction, which in the CyberZoo setup translates to the drone holding a fixed position, as an equilibrium state is achieved between the lateral force generated by the motors and the restorative gravitational force of the pendulum setup.

4.3. Horizontal velocity estimation during spin

The CyberZoo experiments showed time and again that the cyclic thrust control strategy could be used to induce lateral movement in a desired direction. Although the efforts in the last few months of the thesis research was focused on troubleshooting the hardware and demonstrate that this strategy could also work in outdoor conditions, some work went into preparing follow up tests that could be carried out in case of successful outdoor tests. If the control strategy had been shown to also work in outdoor conditions, the next step would have been to attempt to control the drone using a feedback control loop instead of feedforward. In order for this to be possible, the horizontal velocity of the drone as it spins and translates would have to be known, on top of the accurate yaw estimation. In the CyberZoo this proved more challenging than simply using the autopilot INS velocity in the X and Y axes, as the rotation added lots of noise due to the high frequency updates from OptiTrack, and the fact that the drone did not spin exactly around the centroid of the OptiTrack rigid body being tracked.

Filtering approaches were constrained by the necessity of being able to run online within the autopilot loop without requiring a large number of initial observations before giving a good estimate. Simple approaches like exponentially weighted moving averages, also known as simple exponential smoothing, could not be tuned to be able to smooth out the oscillations in the data due to the rotation, while also being able to follow quick changes in the data as the drone's speed changed. These properties of the INS velocity data, the oscillations and quick changes, had to be included in the smoothing approach, and as a result triple exponential smoothing, also known as the Holt-Winters method, was chosen as the filtering method, as it is designed to be able to capture both trend and periodicity of the data. This method is in essence a recursive application of exponential smoothing, with each recursion level containing a different hyper-parameter that has to be tuned to the data. The (additive) Holt-Winters method is given by:

$$s_0 = x_0 \tag{4.1}$$

$$s_t = \alpha(x_t - c_{t-L}) + (1-\alpha)(s_{t-1} + b_{t-1}) \tag{4.2}$$

$$b_t = \beta(s_t - s_{t-1}) + (1-\beta)b_{t-1} \tag{4.3}$$

$$c_t = \gamma(x_t - s_{t-1} - b_{t-1}) + (1-\gamma)c_{t-L} \tag{4.4}$$

Where x_t is the observation, s_t represents the smoothed observation, b_t the trend factor, and c_t the seasonal index at time t. The hyper-parameters $\alpha(0 \leq \alpha \leq 1)$, $\beta(0 \leq \beta \leq 1)$, and $\gamma(0 \leq \gamma \leq 1)$ are the data smoothing factor, trend smoothing factor, and seasonal smoothing factor respectively. The seasonal indices are defined for $i = 1, 2, ..., L$ with L representing the seasonal cycle length. L is a property of the data, which in this application corresponded to the number of samples observed during a full rotation, which depends on the rotational velocity and thus not constant, but an approximate value was computed using 1400 deg/s.

Figure 4.7 shows the application of the Holt-Winters method on the INS velocity data, compared to two exponential smoothing filters for two different values of α. It can be seen that single exponential smoothing is either not sufficiently smoothing the oscillations in the data or

not correctly following sudden changes in the value of the data, while the Holt-Winters estimate can perform both with a delay of only half a rotation. CyberZoo experiments demonstrated that with this method a good estimation of horizontal velocity could be achieved after only 1-2 seconds of the filter being initialized. The application of this method for outdoor test flights would likely be either unnecessary or require different parameters, as the INS data would rely on GPS updates being received at a much lower frequency than the 360 Hz of OptiTrack. Nevertheless, a reliable estimate of the horizontal velocity in the CyberZoo is essential for any future tests of an autonomous controller conducted within the facility.

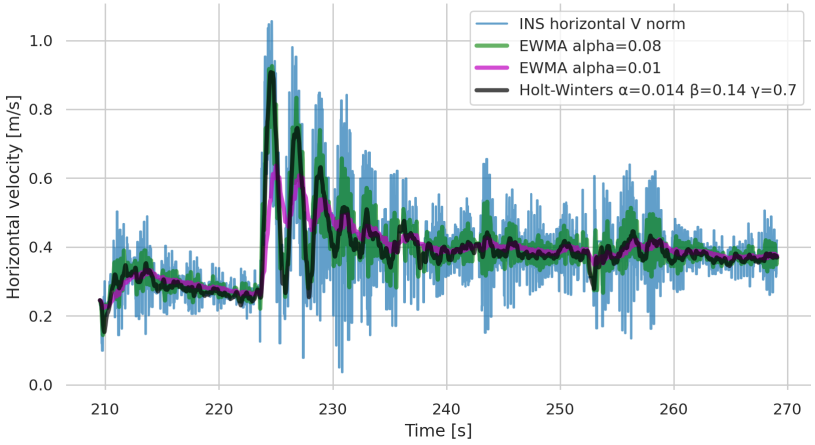

Figure 4.7: Comparison of filter performance on INS horizontal velocity data between an exponentially weighted moving average with two different settings and Holt-Winters smoothing.

4.4. Magnetometer yaw ψ estimation

The cyclic thrust control strategy heavily relied on accurate high frequency estimate of the yaw during rotation originating from the RM3100 magnetometer. This sensor was first tested indoors in the CyberZoo experimental setup, to low degree of success. The yaw estimate was unusable for the control strategy, especially during the cyclic actuation of the motors. The problem persisted even after physically moving the sensor as far away from other electrical components as possible. After many debugging tests, the problem was identified in the transformation of the magnetometer data from the body coordinate frame to the control coordinate

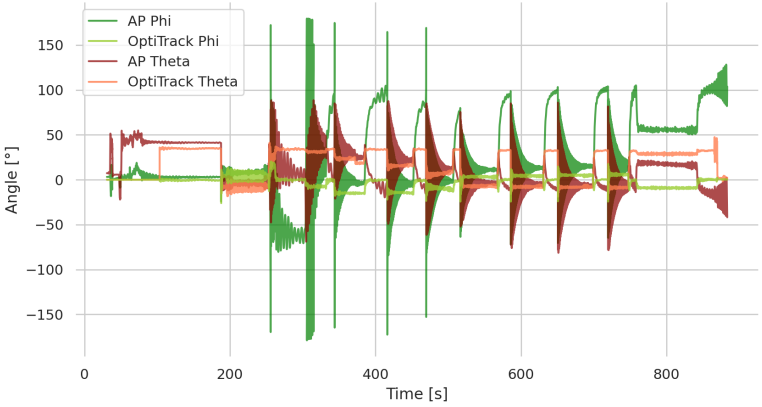

Figure 4.8: Phi and Theta attitude angles estimated by the autopilot (AP) and the true Phi and Theta angles as measured by OptiTrack.

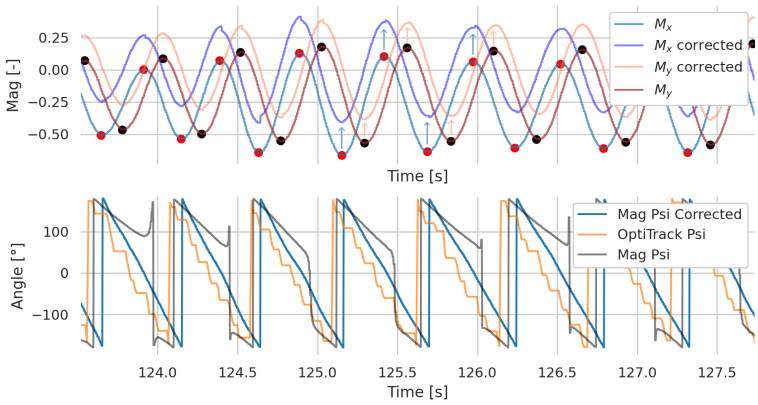

Figure 4.9: Estimation of Psi (yaw) angle using magnetometer data with and without offset correction. The top graph shows the detected peaks and troughs of magnetometer X-axis (M_x) and Y-axis (M_y) data and the corrected X-axis and Y-axis data, shifted by the sinusoid average computed with each period's peak and trough. The bottom graph shows the resulting Psi angle calculated from the arctangent of the Y-axis and X-axis magnetometer data and OptiTrack ground truth. Both graphs illustrate the same time interval.

frame, from which the yaw can then be computed. Large errors in the autopilot roll and pitch estimate were being fed into the transformation matrices. Figure 4.8 shows just how wrong these estimates were, compared to the ground truth calculated by the OptiTrack system.

It is still unclear exactly why the errors in the autopilot estimate were so large. Certainly, the spin maneuver pushes all the sensors involved in the attitude estimation to the limit, with very high sustained rotational velocities of up to 1800-2000 deg/s. Another issue was that very little work went into the optimal way to perform state estimation, as for the majority of the project the focus centered around yaw estimation, which for the most part relied upon very accurate data sources (like OptiTrack). Since no theoretical model of the dynamics of the maneuver existed, it was also very difficult to design a state estimation method that could correctly model the forces that dominate the motion. One of the attempts that was made to improve the state estimation was to switch from a complementary filter to the Extended Kalman filter of Paparazzi. Unfortunately, the Paparazzi code was at the time not working correctly for fixed wing drones, and a quicker solution than to debugging this part of the autopilot software was needed.

In the end, an engineering hack was developed in order to be able to extract an accurate yaw estimate from the magnetometer without needing any additional information from the drone's state. This was achieved by identifying that during rotations with a flat rotational plane, when the magnetometer yaw estimate worked correctly, the magnetometer readings of the X and Y axis oscillated around zero, while when the rotational plane is tilted, which would normally require a coordinate frame transformation using roll and pitch, the oscillations occurred around some other value. If this offset between zero and the average of these offset sinusoidal readings could be calculated (online and in real time), the offset could be corrected and accurate and consistent yaw values could be estimated. Correcting the offset does not normally produce the same results as a transformation matrix, which correctly scales the values, but since the yaw is computed from the arctan of the magnetometer X and Y value only their correct ratio and and sign was necessary.

Using the first derivative of the magnetometer X and Y data, the peaks and troughs were identified and their average calculated in real time, which was then used to correct the magnetometer readings to compute the yaw value. Figure 4.9 illustrates the inner working of this method. In the top figure, the peaks and troughs were determined (in the graph shown with

red and black dots for the magnetometer X-axis and Y-axis respectively), and the sinusoidal shapes shifted upwards so that their average is zero. Discontinuities in the corrected M_x and M_y values can be seen as new peaks or troughs were found and a new average calculated. In the bottom figure the result of the offset correction is shown. The ground truth of the Opti-Track data is shown next to the value of yaw computed using the arctangent of the Y-axis and X-axis of the magnetometer with and without offset correction. The shape of the corrected yaw estimate follows the ground truth significantly better than for the unusable uncorrected values, and while it demonstrates a small phase difference the most important aspect of it is that this phase difference stays constant in time, which for the cyclic thrust control strategy translates to the drone always actuating the motors at the same rotation azimuth.

5
Preliminary Outdoor Test Flights

In order to work towards demonstrating that a conventional flying wing can be controlled in outdoor conditions while undergoing a powered flat spin, a number of preliminary flight tests were conducted to understand whether the sensors were capable of measuring the important state variables, test the hardware, and begin to understand the motion and the major challenges that would need to be tackled.

5.1. Preliminary flight tests

The primary goal of the preliminary flight tests in the initial phase of the thesis was to investigate some key characteristics of the motion, as well as test the suitability of the hardware to reliably reproduce the powered flat spin and measure all the relevant data. Many of the hardware changes discussed in Chapter 3 resulted from the outcome of these tests. From the data collected during these experiments, three spin tests were selected and are showcased in Figures 5.1 to 5.3. The first two figures illustrate an overview of the data logged during a stable flat spin, while the last figure shows a log of an unsuccessful test where the drone did not enter a stable flat spin.

A flat spin is deemed to be stable when the attitude of the rotation plane remains approximately constant and close to parallel to the ground plane. As shown by Figures 5.1 and 5.2 this is characterized by very high rotational velocity of the z axis of the plane that remains constant over time, indicating that the rotation axis does not drastically change direction over the course of the spin and, due to how the IMU was aligned on the drone, that the platform is rotating in the X-Y plane in Body Frame. During the preliminary experiments, the rotational velocities experienced during a stable spin ranged from 1000 to 1500 deg/s, corresponding to 2.8 and 4.2 rotations per second respectively. In Figure 5.2 the accelerometer can be seen to saturate after experiencing accelerations over 16G, its highest detectable value, due to the high rotational velocity. In following flight tests the position of the IMU was changed to be as close to the center of rotation as possible to reduce the risk of saturation, and ultimately led to the decision to rely purely on the RM3100 magnetometer sensor for yaw angle estimation.

In both Figures 5.1 and 5.2 the drone achieved a descent rate of around 5 m/s, even though the rotational velocity of the spin varied by 500 deg/s. It was originally expected that a larger rotational velocity would lead to a lower descent speed, as more lift would be generated from the quicker rotation of the wings. The data instead indicated that the platform was not slowing its descent due to lift generation but primarily due to drag, and that a high rotational velocity would be beneficial only in terms of gyroscopic stability as a result of the larger inertial forces.

Figure 5.3 shows instead the data collected during an unsuccessful spin experiment. An unstable spin is characterized by rotational velocities on multiple axes of the gyroscope, indicating a rotation axis not aligned with the Body z axis, and of significantly lower magnitude than the rotations speeds achieved during stable spins. The resulting descent rate is also twice as high as for a stable spin, unacceptably large for a landing maneuver, and the quickly changing attitude of the rotational plane makes it impossible to apply the relatively simple control strategy discussed in the thesis article.

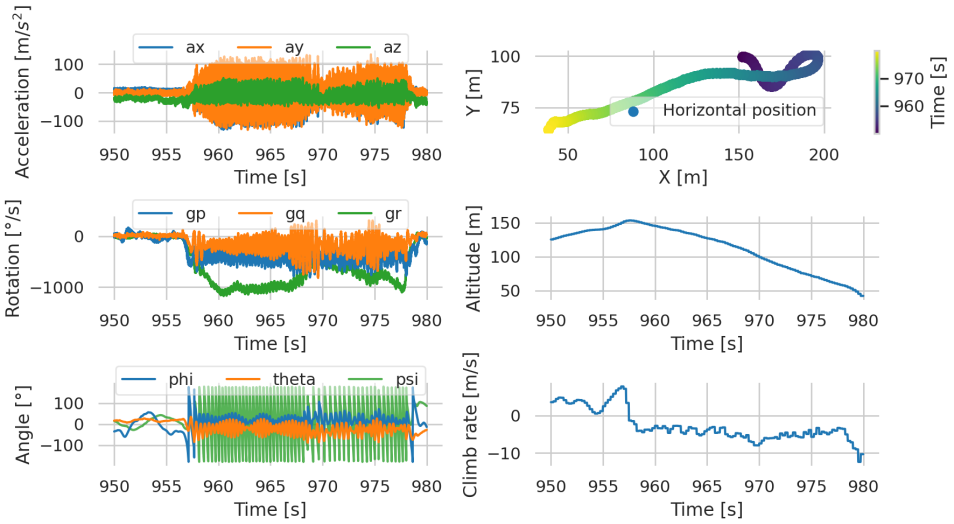

Figure 5.1: Overview of data collected during a stable powered flat spin.

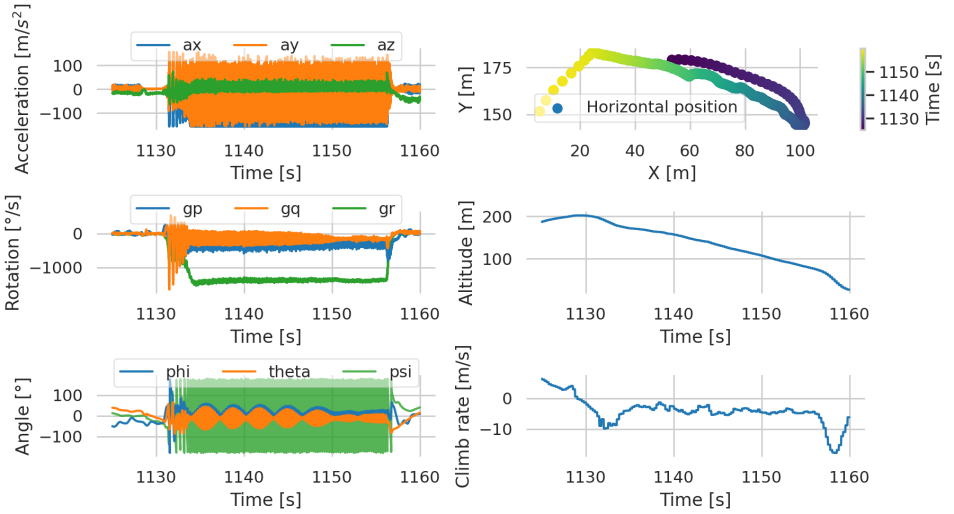

Figure 5.2: Overview of data collected during a stable powered flat spin.

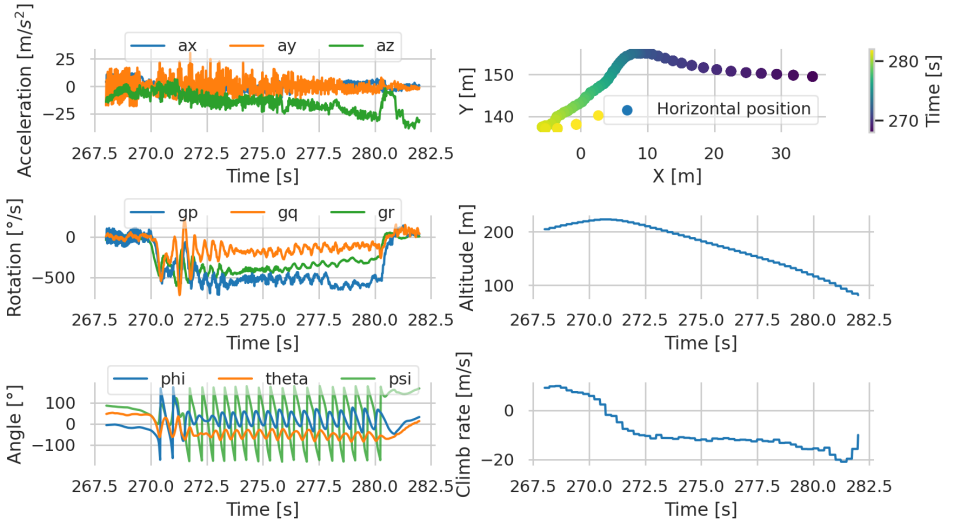

Figure 5.3: Overview of data collected during an unstable powered flat spin.

Bibliography

[1] R. A. Norberg, *Autorotation, self-stability, and structure of single-winged fruits and seeds (samaras) with comparative remarks on animal flight,* Biological Reviews **48**, 561 (1973).

[2] A. Rosen and D. Seter, *Vertical autorotation of a single-winged samara,* Journal of Applied Mechanics **58**, 1064 (1991).

[3] M. R. A. Nabawy and W. J. Crowther, *The role of the leading edge vortex in lift augmentation of steadily revolving wings: a change in perspective,* Journal of the Royal Society Interface **14** (2017), 10.1098/rsif.2017.0159.

[4] S. K. H. Win, L. S. T. Win, G. S. Soh, and S. Foong, *Design modeling and control of collaborative samara autorotating wings (saw),* International Journal of Intelligent Robotics and Applications **3**, 144 (2019).

[5] J. E. Low, L. T. S. Win, J. L. Lee, G. S. Soh, and S. Foong, *Towards a stable three-mode transformable hovering rotorcraft (thor),* in *IEEE/ASME International Conference on Advanced Intelligent Mechatronics* (2018).

[6] E. R. Ulrich, D. J. Pines, and J. S. Humbert, *From falling to flying: the path to powered flight of a robotic samara nano air vehicle,* Bioinspiration and Biomimetics **5**, 1 (2010).

[7] C. E. Thorne and M. Yim, *Design and analysis of a gyroscopically controlled micro air vehicle,* Journal of Intelligent & Robotic Systems **65**, 417 (2012).

[8] A. Konert and T. Dunin, *A harmonized european drone market? – new eu rules on unmanned aircraft systems,* Advances in Science, Technology and Engineering Systems **5**, 93 (2020).

[9] SESAR, *European Drones Outlook Study*, Tech. Rep. (European Union, 2016).

[10] Y. Mulgaonkar, M. Whitzer, B. Morgan, C. Kroninger, A. Harrington, and V. Kumar, *Power and weight considerations in small, agile, quadrotors,* in *Proceedings of SPIE - The International Society for Optical Engineering* (2014).

[11] S. Watkins, J. Burry, A. Mohamed, M. Marino, S. Prudden, A. Fisher, N. Kloet, T. Jakobi, and R. Clothier, *Ten questions concerning the use of drones in urban environments,* Building and Environment **167** (2019), 10.1016/j.buildenv.2019.106458.

[12] J. Winslow, M. Benedict, V. Hrishikeshavan, and I. Chopra, *Design, development, and flight testing of a high endurance micro quadrotor helicopter,* International Journal of Micro Air Vehicles **8**, 155 (2016).

[13] R. Pfeifer, M. Lungarella, and F. Iida, *Self-organization, embodiment, and biologically inspired robotics,* Science **318**, 1088 (2007).

[14] Y. Zou, W. Zhang, and Z. Zhang, *Liftoff of an electromagnetically driven insect-inspired flapping-wing robot,* IEEE Transaction on Robotics **32**, 1285 (2016).

[15] X. Yan, M. Qi, and L. Lin, *Self-lifting artificial insect wings via electrostatic flapping actuators,* in *28th IEEE International Conference on Micro Electro Mechanical Systems (MEMS)* (2015).

[16] K. Meng, W. Zhang, W. Chen, H. Li, P. Chi, C. Zou, X. Wu, F. Cui, W. Liu, and J. Chen, *The design and micromachining of an electromagnetic mems flapping-wing micro air vehicle,* Microsystem Technologies **18**, 127 (2011).

[17] A. Bontemps, T. Vanneste, J. Paquet, T. Dietsch, S. Grondel, and E. Cattan, *Design and performance of an insect-inspired nano air vehicle,* Smart Materials and Structures **22** (2013), 10.1088/0964-1726/22/1/014008.

[18] J. A. Roll, B. Cheng, and X. Deng, *An electromagnetic actuator for high-frequency flapping-wing microair vehicles,* IEEE Transaction on Robotics **31** (2015), 10.1109/TRO.2015.2409451.

[19] L. Hines, D. Campolo, and M. Sitti, *Liftoff of a motor-driven, flapping-wing microaerial vehicle capable of resonance,* IEEE Transaction on Robotics **30**, 220 (2013).

[20] M. Keennon, K. Klingebiel, H. Won, and A. Andriukov, *Development of the nano hummingbird: a tailless flapping wing micro air vehicle,* in *50th AIAA Aerospace Sciences Meeting* (2012).

[21] G. C. H. E. de Croon, K. M. E. de Clercq, R. Ruijsink, B. Remes, and C. de Wagter, *Design, aerodynamics and vision-based control of the delfly,* International Journal of Micro Air Vehicles **1**, 71/97 (2009).

[22] V. Arabagi, L. Hines, and M. Sitti, *Design and manufacturing of a controllable miniature flapping wing robotic platform,* The International Journal of Robotics Research **31**, 785 (2012).

[23] R. Wood, *The first takeoff of a biologically inspired at-scale robotic insect,* IEEE Transaction on Robotics **24**, 341 (2008).

[24] H. Pijnacker, B. J. Scherper, and G. C. H. E. de Croon, *Vertical landing of micro air vehicles using event-based optical flow,* Journal of Field Robotics **35**, 69 (2017).

[25] D. Floreano and R. J. Wood, *Science, technology and the future of small autonomous drones,* Nature **521**, 460 (2015).

[26] D. Seter and A. Rosen, *Stability of the vertical autorotation of a single-winged samara,* Journal of Applied Mechanics **59**, 1000 (1992).

[27] C. W. McCutchen, *The spinning rotation of ash and tulip tree samaras,* Science **197**, 691 (1997).

[28] H. J. Lugt, *Autorotation,* Annual Review Fluid Mechanics **15**, 123 (1983).

[29] A. Azuma and K. Yasuda, *Flight performance of rotary seeds,* Journal of Theoretical Biology **138**, 23 (1989).

[30] K. Yasuda and A. Azuma, *The autorotation boundary in the flight of samara,* Journal of Theoretical Biology **185**, 313 (1997).

[31] E. R. Ulrich and D. J. Pines, *Effects of planform geometry on mechanical samara autorotation efficiency and rotational dynamics,* Journal of the American Helicopter Society **57**, 1 (2012).

[32] J. R. Usherwood and C. P. Ellington, *The aerodynamics of revolving wings i. model hawkmoth wings,* Journal of Experimental Biology **205**, 1547 (2002).

[33] C. P. Ellington, C. van der Berg, A. P. Willmott, and A. L. R. Thomas, *Leading-edge vortices in insect flight,* Nature **384**, 626 (1996).

[34] D. Lentink, W. B. Dickson, J. L. vanLeeuwen, and M. H. Dickinson, *Leading-edge vortices elevate lift of autorotating plant seeds,* Science **324**, 1438 (2009).

[35] J. M. Birch and M. H. Dickinson, *Spanwise flow and the attachment of the leading-edge vortex on insect wings,* Nature **412**, 729 (2001).

[36] E. Limacher and D. E. Rival, *On the distribution of leading-edge vortex circulation in samara-like flight,* Journal of Fluid Mechanics **776**, 316 (2015).

[37] E. Limacher and D. E. Rival, *On the distribution of leading-edge circulation in samara-like flight,* Journal of Fluid Mechanics **776**, 316 (2015).

[38] D. Lentink and M. H. Dickinson, *Rotational accelerations stabilize leading edge vortices on revolving fly wings,* Journal of Experimental Biology **212**, 2705 (2009).

[39] E. Limacher, C. Morton, and D. Wood, *On the trajectory of leading-edge vortices under the influence of coriolis acceleration,* Journal of Fluid Mechanics **800** (2016), 10.1017/jfm.2016.395.

[40] T. Jardin and L. David, *Coriolis effect enhance lift on revolving wings,* Physical Review **91** (2015), 10.1103/PhysRevE.91.031001.

[41] J. R. Usherwood and C. P. Ellington, *The aerodynamics of revolving wings ii. propeller force coefficients from mayfly to quail,* Journal of Experimental Biology **205**, 1565 (2002).

[42] K. Varshney, S. Chang, and Z. J. Wang, *The kinematics of falling maple seeds and the initial transition to a helical motion,* Nonlinearity **25** (2011), 10.1088/0951-7715/25/1/C1.

[43] I. Lee and H. Choi, *Scaling law for the lift force of autorotating falling seeds at terminal velocity,* Journal of Fluid Mechanics **835**, 406 (2017).

[44] M. Y. Zakaria, C. R. dos Santos, A. Dayhoum, F. D. Marques, and M. R. Hajj, *Modeling and prediction of aerodynamic characteristics of free fall rotating wing based on experiments,* in *18th International Conference on Aerospace Sciences and Aviation Technology* (2019).

[45] L. W. Traub, *Analysis and estimation of the lift components of hovering insects,* Journal of Aircraft **41**, 284 (2004).

[46] D. Rezgui, I. H. Arroyo, and R. Theunissen, *Model for the sectional leading-edge vortex lift prediction of rotating samara seeds performance,* The Aeronautical Journal **124**, 1 (2020).

[47] C. Hockley and B. Butka, *The samareye: A biologically inspired autonomous vehicle,* in *29th Digital Avionics Systems Conference* (2010).

[48] E. Ulrich, D. J. Pines, and S. Gerardi, *Autonomous flight of a samara mav,* in *American Helicopter Society 65th Annual Forum* (2009).

[49] E. Ulrich, J. S. Humbert, and D. J. Pines, *Pitch and heave control of robotic samara micro air vehicles,* Journal of Aircraft **47**, 1290 (2010).

[50] S. Gerardi, E. Ulrich, J. S. Humbert, and D. Pines, *Hover stabilization of a controllable mechanical samara,* in *AIAA Guidance, Navigation, and Control Conference* (2010).

[51] E. Ulrich, J. Grauer, D. J. Pines, J. Hubbard, and J. S. Humbert, *Identification of a robotic samara aerodynamic/multi-body dynamic model,* in *AIAA Atmospheric Flight Mechanics Conference* (2010).

[52] D. J. Pines, J. S. Humbert, J. E. Hubbard, E. R. Ulrich, I. Faruque, and J. Grauer, *Control model for robotic samara: dynamics about a coordinated helical turn,* Journal of Guidance, Control, and Dynamics **33**, 1921 (2010).

[53] M. Orsag, J. Cesic, T. Haus, and S. Bogdan, *Spincopter wing design and flight control,* Journal of Intelligent & Robotic Systems **70**, 165 (2012).

[54] L. S. T. Win, S. K. H. Win, D. Sufiyan, G. S. Soh, and S. Foong, *Achieving efficient controlled flight with a single actuator,* in *IEEE/ASME International Conference on Advanced Intelligent Mechatronics* (2020).

[55] S. Bai and P. Chirarattananon, *Design and take-off flight of a samara-inspired revolving-wing robot,* in *IEEE/RSJ International Conference on Intelligent Robots and Systems (IROS)* (2019).

[56] B. Jung and D. Rezgui, *Investigating the autorotational performance of a scaled samara rotor in vertical and forward flight,* in *42nd European Rotorcraft Forum* (Association Aeronautique et Astronautique de France, 2017).

[57] K. Fregene, D. Sharp, C. Bolden, J. King, C. Stoneking, and S. Jameson, *Autonomous guidance and control of a biometric single-wing mav,* (2011), lockheed Martin Advanced Technology Laboratories.

[58] S. Jameson, K. Fregene, M. Chang, N. Allen, H. Youngren, and J. Scroggins, *Lockheed martin's samarai nano air vehicle: challenges, research, and realization,* in *50th AIAA Aerospace Sciences Meeting Including the New Horizons Forum and Aerospace Exposition* (2012).

[59] J. E. Low, L. T. S. Win, D. S. B. Shaiful, C. H. Tan, G. S. Soh, and S. Foong, *Design and dynamic analysis of a transformable hovering rotorcraft (thor),* in *IEEE International Conference on Robotics and Automation* (2017).

[60] J. E. Low, D. Sufiyan, L. T. S. Win, G. S. Soh, and S. Foong, *Design of a hybrid aerial robot with multi-mode structural efficiency and optimized mid-air transition,* Unmanned Systems **7**, 195 (2019).

[61] G. Matič, M. Topič, and M. Jankovec, *Mathematical model of a monocopter based on unsteady blade-element momentum theory,* Journal of Aircraft **52**, 1905 (2015).

[62] M. E. Dormiyani, A. Banazadeh, and F. Saghafi, *Multibody modeling and simulation of monocopter micro air vehicle,* Applied Mechanics and Materials **772**, 401 (2015).

[63] M. Ezabadi, M. H. Sabeti, and A. Banazadeh, *Dynamics identification of a monocopter using neural networks,* International Journal of Modeling and Optimization **7**, 179 (2017).

[64] H. T. Siegelmann, B. G. Horne, and C. L. Giles, *Computational capabilities of recurrent narx neural networks,* IEEE Transactions on Systems, Man, and Cybernetics **27**, 208 (1997).

[65] B. Obradovic, G. Ho, R. Barto, K. Fregene, and D. Sharp, *A multi-scale simulation methodology for the samarai monocopter μuav,* in *AIAA Modeling and Simulation Technologies Conference* (2012).

[66] B. Malik, S. Akhtar, and J. Masud, *Dynamic analysis and nonlinear simulation of aircraft flat spin,* Journal of the Chinese Institute of Engineers **40**, 471 (2017).

[67] B. Malik, S. Akhtar, and J. Masud, *Aircraft spin characteristics with high-alpha yawing moment asymmetry,* in *Institutions of Mechanical Engineers, Journal of Aerospace Engineers* (2017).

[68] S. Akhtar, B. Malik, and J. Masud, *Control law affect on spin characteristics of aerodynamically asymmetric aircraft,* in *AIAA Atmospheric Flight Mechanics Conference* (2017).

[69] D. Kim, G. Oh, Y. Seo, and Y. Kim, *Flat spin recovery for unmanned aerial vehicle,* Journal of Guidance, Control, and Dynamics **40**, 1074 (2017).

[70] M. W. Mueller and R. D'Andrea, *Stability and control of a quadcopter despite complete loss of one, two, or three propellers,* in *IEEE International Conference on Robotics and Automation (ICRA)* (2014).

[71] M. W. Mueller and R. D'Andrea, *Relaxed hover solutions for multicopters: application to algorithmic redundancy and novel vehicles,* International Journal of Robotics Research **35**, 873 (2016).

[72] P. Lu and E. vanKampen, *Active fault-tolerant control for quadrotors subjected to a complete rotor failure,* in *IEEE/RSJ International Conference on Intelligent Robots and Systems (IROS)* (2015).

[73] S. Sun, L. Sijbers, X. Wang, and C. deVisser, *High-speed flight of a quadrotor despite loss of single rotor,* IEEE Robotics and Automation Letters **3**, 3201 (2018).

[74] S. Higashino and K. Nakama, *Vertical landing of a fixed-wing uav using the flat spin,* in *31st Congress of the International Council of the Aeronautical Sciences, ICAS* (2018).

[75] S. K. H. Win, L. S. T. Win, G. S. Soh, and S. Foong, *Design optimization of flap configuration in samara autorotating wing with multi-functional aerodynamic structure,* in *IEEE/ASME International Conference on Advanced Intelligent Mechatronics* (2019).

[76] S. K. H. Win, D. Sufiyan, L. S. T. Win, G. S. Soh, and S. Foong, *Design optimization of flap configuration in samara autorotating wing with multi-functional aerodynamic structure,* in *IEEE/ASME International Conference on Advanced Intelligent Mechatronics* (2019).

[77] J. Mitchell and J. A. Marshall, *Towards a novel auto-rotating lidar platform for cavity surveying,* Tunnelling and Underground Space Technology **97**, 1 (2020).

[78] V. Nadal-Mora and A. Sanz-Andres, *Stability analysis of a free-falling pararotor,* Journal of Aircraft **43**, 980 (2006).

[79] V. Nadal-Mora, A. Sanz-Andres, and A. Cuerva, *Model of the aerodynamic behavior of a pararotor,* Journal of Aircraft **43**, 1893 (2006).

[80] J. Piechocki, V. Nadal-Mora, and A. Sanz-Andres, *Numerical simulation of pararotor dynamics: effects of mass displacement from blade plane,* Aerospace Science and Technology **55**, 400 (2016).

[81] H. Youngren, S. Jameson, and B. Satterfield, *Design of the samarai monowing rotorcraft nano air vehicle,* in *American Helicopter Society* (American Helicopter Society International, 2009).

[82] M. Samani, M. Tafreshi, I. Shafieenejad, and A. A. Nikkhah, *Minimum-time open-loop and closed-loop optimal guidance with ga-pso and neural fuzzy for samarai mav flight,* IEEE Aerospace and Electronic Systems Magazine **30**, 28 (2015).

Appendix A
Relevant Videos

Samarai Lockheed Martin [57, 81, 82]
https://www.youtube.com/watch?v=Pbegin59K6s
https://www.youtube.com/watch?v=5LqSWiatV0Q
https://www.youtube.com/watch?v=n_q_DD_4LNg

THOR Singapore University of Technology and Design [59]
https://www.youtube.com/watch?v=EPQdIDy2atY

Samara monocopter University of Maryland [6, 31, 48–52]
https://www.youtube.com/watch?v=sbuGCgc-JCM
https://www.youtube.com/watch?v=u23Hqq8QbeE

SAW Singapore University of Technology and Design [4, 75, 76]
https://www.youtube.com/watch?v=6D0yzQjINEw
https://www.youtube.com/watch?v=fv57Ffrih2o
https://www.youtube.com/watch?v=B74ovD-iJCU

RC Enthusiasts flat spin maneuvers
https://www.youtube.com/watch?v=AvBobSj2K4g
https://www.youtube.com/watch?v=H3M04wVK9fE
https://www.youtube.com/watch?v=2_qSqhAvxoQ
https://www.youtube.com/watch?v=oJ-Gb9rPoqg
https://www.youtube.com/watch?v=CZ8vmclk1H8
https://www.youtube.com/watch?v=6rhuiJZC86c
https://www.youtube.com/watch?v=D7KaWTMgOM4
https://www.youtube.com/watch?v=U2WNabLIf9E